The Chiral Restoration Transition of QCD and Low Mass Dileptons

R. Rapp[1], J. Wambach[2] and H. van Hees[3]
[1]Cyclotron Institute and Physics Department, Texas A&M University,
College Station, TX 77843-3366, U.S.A.
[2] TU Darmstadt, Schloßgartentr. 9, D-64289 Darmstadt, Germany
[3] Institut für Theoretische Physik, Justus-Liebig-Universität Giessen,
Heinrich-Buff-Ring 16, D-35392 Giessen, Germany

January 21, 2009

Abstract

Recent developments in the evaluation of vector-meson spectral functions in hot and dense matter are discussed with emphasis on connections to the chiral phase transition in QCD. Model independent approaches including chiral low-density expansions, lattice QCD, chiral and QCD sum rules are put into context with model predictions for in-medium vector-spectral function utilizing effective Lagrangians. Hadronic many-body calculations predict a strong broadening (and little mass shift) of the ρ spectral function which rapidly increases close to the expected phase boundary of hadronic and quark-gluon matter. Pertinent dilepton rates appear to degenerate with perturbative quark-antiquark annihilation in the Quark-Gluon Plasma, suggestive for chiral symmetry restoration. Applications to low-mass dilepton spectra in heavy-ion collisions result in quantitative agreement with recent high-quality data at the CERN-SPS. Thermal radiation from temperatures around T_c consistently reproduces the experimental dilepton excess observed at masses above 1 GeV as well. The interpretation of dilepton sources at high transverse momentum appears to be more involved.

Published in: Landolt-Brnstein **23**, 134 (2010),
DOI: 10.1007/978-3-642-01539-7_6
Preprint: arXiv:0901.3289v1 [hep-ph]

Contents

1 Introduction

The quest for the elementary entities of matter has always been a central objective in physics. Of no less interest is the emergence of the structure (or phases) of matter built from its basic constituents and their interactions. The exploration of matter governed by the strong force is at the forefront of contemporary research in nuclear physics. The most common form of strongly interacting matter in the present-day universe is contained in atomic nuclei, which are bound states of nucleons, i.e., protons and neutrons. Nuclear matter as found in the center of heavy nuclei is characterized by a nucleon (energy) density of about $\varrho_0 = 0.16\,\mathrm{fm}^{-3}$ ($\varepsilon_0 = 0.15\,\mathrm{GeV/fm}^3$), rendering one table spoon of this material a mass of about one million kilotons ($10^{12}\,\mathrm{kg}$). The binding of nucleons is strong enough to cause a reduction of nuclear masses by about 1% compared to the sum of the rest mass of the individual nucleons, $m_N \simeq 940\,\mathrm{MeV}/c^2$. But how does the mass of a nucleon arise? In the late 1960's it was discovered that the nucleon itself is a composite object, built of three "valence" quarks of *up* (u) and *down* (d) "flavor". The bare masses of u and d quarks are only about 5-10 MeV/c^2, and believed to be generated by a condensate of (yet to be discovered) Higgs bosons in the electroweak (EW) sector of the Standard Model of Elementary Particles. That is, about 98% of the nucleon's mass is generated dynamically by the strong interaction. Moreover, no individual quarks have been observed in nature thus far: they are "confined" into hadrons, either baryons or mesons (conglomerates of three valence quarks or of a quark and antiquark, respectively). In the 1970's, the quantum field theory underlying the strong force has been developed, Quantum Chromodynamics (QCD), based on quarks and gluons as fundamental degrees of freedom. This theory has been quantitatively confirmed in high-energy scattering experiments, where the strong coupling constant, $\alpha_s \simeq 0.1$, is relatively small and perturbation theory can be reliably utilized to obtain quantitative results for observables. However, at low momentum transfers, α_s becomes large, perturbation theory ceases to be applicable and nonperturbative mechanisms take over. It is in this regime where quark confinement and mass generation occur, posing formidable challenges for their theoretical understanding [1].

1.1 QCD Vacuum and Chiral Restoration

It turns out that confinement and mass generation are intimately connected with the phase structure of strongly interacting matter (see, e.g., Ref. [2]). In fact, even the structure of the QCD vacuum is far from trivial: similar to the EW sector, it is believed to be filled with condensates, which are closely related to the origin of hadronic masses. There are, however, important differences: the QCD condensates are made of (scalar) composites of quarks and gluons (rather than elementary fields like the Higgs boson), and they do not induce a breaking of the gauge symmetry. In what follows, the so-called "chiral" quark-antiquark condensate, $\langle 0|\bar{q}q|0\rangle \simeq (-250\,\mathrm{MeV})^3$, will be of particular importance. It breaks the (approximate) chiral symmetry of QCD, which corresponds to the conservation of left and right "handedness" of massless quarks (applicable for the light u and d quarks, whose masses are parametrically small, $m_{u,d} \ll |\langle 0|\bar{q}q|0\rangle|^{1/3}$). While the quark condensate cannot be directly observed, its consequences are apparent in the excitations of the condensed ground state, i.e., in the hadron spectrum. Since chiral symmetry is a global symmetry (rather than a local one depending on space-time position), its spontaneous breaking must be accompanied by (almost) massless Goldstone bosons. For two quark flavors the latter are identified with the three charge states of the pion, whose mass, $m_\pi \simeq 140\,\mathrm{MeV}$, is

"abnormally" small compared to that of all the other hadrons (e.g., $m_N \simeq 940\,\mathrm{MeV}$). The observed hadron spectrum encodes further evidences for the spontaneous breaking of chiral symmetry (SBχS): chiral multiplets (e.g., $\rho(770)$-$a_1(1260)$ or $N(940)$-$N^*(1535)$), which would be degenerate if the ground state were chirally symmetric, exhibit a large mass splitting of typically $\Delta M \simeq 500\,\mathrm{MeV}$. The effects of SB$\chi$S seem to (gradually) cease as one goes up in mass in the hadronic spectrum [3]. This is one of the indications that SBχS is a low-energy, strong-coupling phenomenon which is no longer operative at high momentum transfers where perturbation theory becomes applicable.

When heating the QCD vacuum its condensate structure is expected to change. Loosely speaking, thermally excited hadrons "evaporate" condensed $\bar{q}q$ pairs which eventually leads to the restoration of the spontaneously broken chiral symmetry. Numerical computations of the lattice-discretized path integral for QCD at finite temperature predict chiral symmetry restoration (χSR) to occur at a (pseudo-) critical temperature of $T_c \simeq 160$-$190\,\mathrm{MeV}$ [4, 5], corresponding to an energy density of about $\varepsilon_c \simeq 1\,\mathrm{GeV/fm^3}$. The chiral transition is characterized by a rapid decrease of the $\bar{q}q$ condensate, which, in fact, serves as an order parameter of strongly interacting matter. In the limit of vanishing light quark masses and for three quark flavors, this transition is of first order, while for realistic quark masses as realized in nature (two light quarks u and d and a more heavy strange quark, $m_s \simeq 120$ MeV), it is more likely a rapid cross-over. Key manifestations of chiral symmetry restoration are its (observable) consequences for the hadron spectrum. Chiral partners must degenerate implying massive medium modifications of hadronic spectral functions as the transition is approached. This notion is a quite general concept found, e.g., in solid state physics where phase transitions are routinely diagnosed utilizing "soft-mode spectroscopy". This applies in particular to a second order phase transition where the mode associated with an order parameter becomes massless (soft). But even for bulk matter properties, rapid changes in the thermodynamic state variables are directly related to changes in the relevant degrees of freedom at the typical thermal scale (temperature or Fermi momentum). Interestingly, the chiral transition is accompanied by the dissolution of hadrons into quarks, i.e., the deconfinement transition, at the same temperature (at least for vanishing net baryon density). The reason for the apparent coincidence of the two transitions is not understood. The deconfined and chirally restored strongly interacting matter is commonly referred to as the Quark-Gluon Plasma (QGP). The experimental verification and theoretical understanding of the mechanisms leading to the QGP are central objectives in modern nuclear research.

1.2 Ultrarelativistic Heavy-Ion Collisions

The only way to produce and study hot and dense strongly interacting matter in the laboratory is by colliding atomic nuclei at high energies. Several large-scale experiments at ultrarelativistic bombarding energies, $E_{\mathrm{lab}} \gg m_N$, have been conducted over the past $\sim$20 years, most recently at the SPS at CERN (at center-of-mass energies up to $\sqrt{s} =$ 17.3 AGeV) and at the Relativistic Heavy-Ion Collider (RHIC) at Brookhaven (up to $\sqrt{s} = 200$ AGeV) [6, 7] with the heaviest available nuclei at A$\simeq$200 (Pb and Au).

The first question that needs to be answered is whether these reactions produce *equilibrated matter*, i.e., do the produced particles undergo sufficient rescattering to justify the notion of an interacting medium characterized by bulk thermodynamic variables? Extensive and systematic measurements of hadronic observables have lead to a positive answer. This is extremely exciting as it puts within grasp the possibility to recreate, at least for a

short moment, the matter which the early universe was made of just a few microseconds after the Big Bang! While hadronic measurements are discussed and interpreted in depth in other contributions of this volume, let us sketch some of their main features: transverse-momentum (p_T) spectra of different hadron species (pions, kaons, protons, etc.), which characterize the hadronic fireball just before break-up at its "thermal freeze-out", exhibit a collective explosion reaching an average speed of about half the speed of light at a final temperature of $T_{\rm fo}^{\rm th} \simeq 100\,{\rm MeV}$. The ratios of the observed hadron species point at a significantly higher temperature of $T_{\rm fo}^{\rm ch} \simeq 160\,{\rm MeV}$ [8, 9], i.e., the chemistry of the fireball (driven by inelastic scattering processes) appears to freeze out significantly earlier than kinetic equilibrium (maintained by elastic interactions). This is consistent with the large difference of empirical elastic (e.g., $\pi\pi \to \rho \to \pi\pi$ or $\pi N \to \Delta \to \pi N$) and inelastic (e.g., $\pi\pi \to K\bar{K}$) hadronic cross sections, with typical values of $\sim$100 mb vs. $\sim$1 mb, respectively. Since the cross sections determine the relaxation times according to $\tau \simeq (\varrho_h \sigma v_{\rm rel})^{-1}$ (ϱ_h: hadron density, $v_{\rm rel}$: relative velocity of the colliding hadrons), one obtains a clear hierarchy in the underlying relaxation times, $\tau_{\rm th} \ll \tau_{\rm ch}$. The interacting hadronic phase between chemical and thermal freeze-out will play an important role in the remainder of this article. More differential analyses of the flow patterns of the measured hadrons allow to trace back the matter properties to earlier times in the evolution of the fireball. In particular, the magnitude of the "elliptic flow" measured at RHIC indicates that the medium thermalizes on a rather short time scale, $\tau \leq$ 1-2 fm/c after initial impact, translating into (energy-) densities of a factor 10 or more above the critical one[1]. A thermal (hydrodynamic) description [10, 11, 12, 13] of the fireball in semi-/central collisions of heavy nuclei at RHIC appears to be valid for hadrons up to momenta of $p_T \simeq$ 2-3 GeV, comprising approximately 95% of all produced particles. At high transverse momenta, $p_T > 5$ GeV, hadron production is dominated by hard scattering, i.e., a primordial parton-parton collision at high momentum transfer within the incoming nucleons, followed by fragmentation into (a spray of) hadrons (jets). In central Au-Au collisions at RHIC, a factor of $\sim$5 suppression of high-p_T hadron production has been observed ("jet quenching")[2]. While these hadrons (or their parent quarks) do not thermalize, their suppression indicates a substantial coupling to the created medium, associated with an energy loss of a fast parton propagating through the fireball. The (energy-) density of the medium required to account for this effect is roughly consistent with the estimate inferred from a hydrodynamic description of the elliptic flow of low-p_T hadrons.

A second level of questions concerns the relevant degrees of freedom of the produced matter, i.e., whether there is explicit evidence that individual partons leave a distinctive footprint in observables. It turns out that the elliptic flow is again revealing interesting features in this context: it has been found [14, 15] that the elliptic-flow coefficient, $v_2^h(K_T)$, of all measured hadrons, h=π, K, p, Λ, Σ, ϕ, ..., exhibits a remarkable universality as a function of transverse kinetic energy, K_T=$m_T - m_h$ (m_T=$(p_T^2$+$m_h^2)^{1/2}$): when scaled with

[1] Elliptic flow characterizes the azimuthal asymmetry in the p_T-spectra of particles (in the plane transverse to the beam axis). In a non-central heavy-ion collision, the initial nuclear overlap (interaction) zone is "almond-shaped". If the system thermalizes before this spatial anisotropy is smeared out (e.g., due to free streaming), a larger pressure gradient builds up along the "short'" compared to the "long" axis of the initial almond. This thermal pressure drives a collective expansion of the "almond" which is stronger along the short axis and thus results in particle momenta with a preference to be aligned with this axis. The magnitude of the elliptic flow is thus sensitive to how fast thermalization is established.

[2] Jet quenching is probably also present at the SPS but it is quantitatively smaller than at RHIC (about a factor of 2 suppression) and masked by a large initial p_T broadening in the interpenetrating nuclei prior to the hard scattering, known as "Cronin effect".

the constituent-quark number content, n_q, of hadron h, all measured hadron-v_2 data appear to collapse on a single curve, $v_2^q(K_t{\equiv}K_T/n_q){=}v_2^h(K_T)/n_q$. This has been interpreted as evidence for a collectively expanding partonic source hadronizing via quark coalescence. A fully consistent theoretical description of this phenomenon has not been achieved yet.

A third level of investigations has to address signals of the deconfinement and/or chiral restoration transitions. In a rigorous sense, this requires the assessment of order parameters associated with these transitions. However, changes in order parameters are not always easily observable. This is particularly true in the present context and we are led back to the idea of "mode spectroscopy", to be conducted in the environment of a short-lived, rapidly expanding fireball of a heavy-ion collision. Individual (stable) hadrons emanating from the collision zone have all long recovered their free (vacuum) masses by the time they are measured in the detectors. A better observable are invariant-mass spectra of short-lived resonance decays, $h \to h_1 h_2$, with a lifetime, τ_h, comparable to, or smaller than, the lifetime of the interacting fireball, $\tau_{\rm FB} \simeq 10$ fm/c. Such a resonance (e.g., $\Delta \to \pi N$ or $\rho \to \pi\pi$) has a large probability to decay inside the medium so that its decay products can carry the information on its invariant-mass, $m_h^2 = (p_1 + p_2)^2$, at the point of decay to the detector. In principle, this would allow to determine the invariant-mass distribution (or spectral function) of the resonance h in the medium. The problem is that the decays products, h_1 and h_2, are likely to undergo further rescattering in the fireball which destroys the desired invariant-mass information. The latter will thus be largely restricted to the dilute (break-up) stages of the medium in a heavy-ion collision.

1.3 Dilepton Spectroscopy

The decisive step to obtain access to hadronic spectral functions in the hot and dense regions of the medium is provided by electromagnetic (EM) probes, i.e., photons (γ) and dileptons (arising from virtual (timelike) photons, $\gamma^* \to l^+l^-$ with $l{=}e$ or μ) [16, 17, 18]. These are not subject to the strong force and thus suffer negligible final-state interactions, with a mean free path which is much larger than the typical size of the fireball, $R_{\rm FB} \simeq 10$ fm. The natural candidates for in-medium spectroscopy are the vector mesons (V), which carry the quantum numbers of the photon (spin-parity $J^P{=}1^-$) and thus directly couple to exclusive dilepton final states, $V \to l^+l^-$. In the low-mass region ($M{\leq}1$ GeV), which is the region of interest to study chiral restoration, the prominent vector mesons are $\rho(770)$, $\omega(782)$ and $\phi(1020)$. In fact, the famous vector dominance model (VDM) [19] asserts that the coupling of a (real or virtual) photon to *any* EM hadronic current exclusively proceeds via an intermediate vector meson (which is excellently satisfied in the mesonic sector but subject to corrections in the baryonic sector). Thus, if VDM holds in hadronic matter, dilepton emission is indeed equivalent to in-medium vector-meson spectroscopy. In thermal equilibrium, the contribution from the (isovector) ρ meson dominates over the ω by a factor of $\sim$10 (factor $\sim$5 over the ϕ, which, however, is thermally suppressed due to its larger mass). Furthermore, it can be shown [20] that, in the context of a heavy-ion collision, low-mass dilepton radiation from the hadronic phase dominates over the emission from a putative QGP phase, even at collider energies (RHIC and LHC)[3]. The excitement (and theoretical activity) in the field was further spurred by the suggestion of Brown and Rho [21] that the ρ-meson mass should drop to (almost) zero

[3]This is due to the much larger three-volume in the hadronic phase; at larger dilepton masses, $M{>}1$ GeV, the thermal Boltzmann factor, $\mathrm{e}^{-q_0/T}$, augments the sensitivity to higher temperatures which increases the QGP contribution relative to the hadronic one in the inclusive dilepton spectrum.

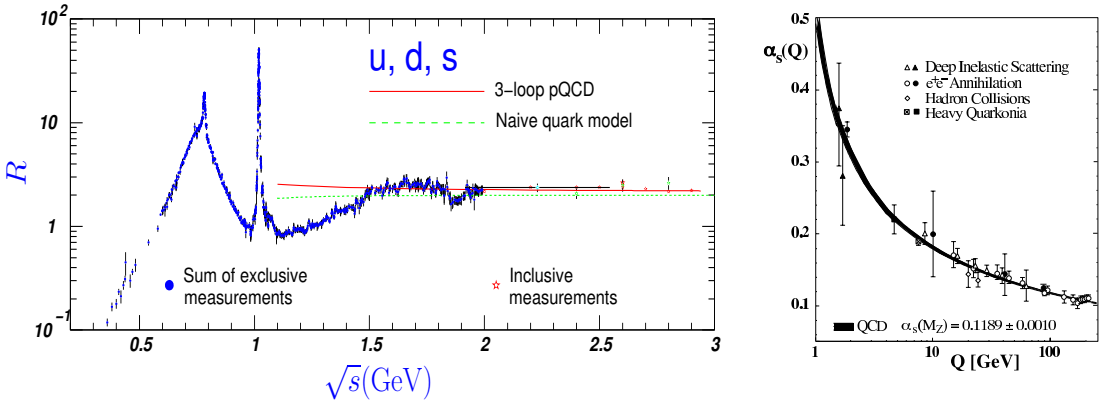

Figure 1: *Left panel: ratio of cross sections, $R=\sigma_{ee\to\text{hadrons}}/\sigma_{ee\to\mu\mu}$, for electron-positron annihilation into hadrons relative to muon-antimuons, as a function of center-of-mass energy, $\sqrt{s}$. The experimental data exhibit a nonperturbative resonance regime up to $\sqrt{s}\simeq 1.1$ GeV, exhausted by the light vector mesons ρ, ω and ϕ, followed by a transition to an almost structureless perturbative regime at $\sqrt{s}\gtrsim 1.5$ GeV. The latter is well described by perturbative QCD (pQCD), especially for $\sqrt{s}\geq 2$ GeV, where residual "oscillations" (due to excited vector resonances) have essentially ceased. The naive quark-model prediction (leading-order pQCD, $\mathcal{O}(\alpha_s^0)$) is given by $R_{QM}=N_c\sum_{q=u,d,s}e_q^2=2$. Right panel: strong coupling constant as a function of momentum transfer [33]; note the increase of α_s toward small Q suggestive for the emergence of nonperturbative phenomena.*

as a consequence of χSR. Early dilepton measurements in S(200 AGeV)-Au collisions at the CERN-SPS by the CERES collaboration [22] found a large enhancement of the spectrum at invariant masses below the nominal ρ mass, i.e., for $M\simeq$0.2-0.7 GeV. These data could be well described by a dropping-mass scenario implemented into relativistic transport models within a mean-field description [23, 24]. Subsequently, more "conventional" medium modifications of the ρ meson were investigated based on its rescattering on constituents of a hadronic medium, see, e.g., Refs. [25, 26, 27, 28] for reviews. The generic finding of these hadronic many-body calculations was a strong broadening of the ρ spectral function, which, when extrapolated to the putative phase transition temperature, $T_c\simeq 175$ MeV, leads to a complete "melting" of the resonance structure [29]. The broadening effect could account for a large part of the low-mass dilepton excess observed in S-Au collisions. The agreement was even better [30] with improved CERES/NA45 measurements carried out in the heavier Pb(158 AGeV)-Au system [31, 32]. The connection of the ρ melting to χSR appeared to be less direct than in dropping-mass scenarios. However, in Refs. [34, 30] it was found that the hadronic dilepton rates following from the "melted" ρ close to T_c rather closely resemble the rates computed in a partonic description, i.e., perturbative quark-antiquark annihilation. In the vacuum, such a phenomenon is well known from the e^+e^- annihilation into hadrons: for $M\geq$1.5 GeV the total cross section is well described within perturbative QCD using quark-antiquark final states, known as "parton-hadron duality", cf. Fig. 1. It was therefore suggested that the conceptual implication of the ρ melting is a reduction of the "duality threshold" [34, 30], from M_{dual}=1.5 GeV in the vacuum to essentially zero around T_c. Note that a "perturbative" dilepton rate automatically implies chiral restoration (i.e., degeneracy of vector and axialvector channels).

The accuracy in the 1995/1996 CERES/NA45 dielectron data [31, 32] did not allow for a decisive experimental discrimination of the dropping-mass and melting-resonance

scenarios. An important step forward was realized with the NA60 dimuon spectra [35] in In(158 AGeV)-In collisions at the SPS. Excellent mass resolution and superior statistics enabled, for the first time, an isolation of the "excess radiation" (by subtraction of final-state hadron decays). The shape of the excess spectrum clearly favors a broadened ρ spectral function over scenarios involving dropping masses. The original predictions of hadronic many-body theory [30, 20] are, in fact, in quantitative agreement [36] with the inclusive mass spectra in semi-/central In-In collisions. In the last round of CERES/NA45 data [37] excess spectra have also been extracted in Pb-Au collisions (by subtraction of final-state hadron decays using a statistical model [8]). While the overall data quality does not reach the level of NA60, the larger collision system and the access to very small dilepton masses in the dielectron channel (dimuons have a threshold of $2m_\mu$=210 MeV) can provide additional insights.

The dilepton program at the CERN-SPS has thus far reached the highest level of maturity in the heavy-ion context. It also included a CERES/NA45 measurement in a low-energy Pb(40 AGeV)-Au run [38], which produced tantalizing hints for an even larger excess than at 158 AGeV, but was unfortunately hampered by low statistics. At much lower, relativistic bombarding energies (1-2 AGeV), the DLS collaboration at the BEVALAC reported a very large dilepton excess [39], which has recently been confirmed by the HADES collaboration at SIS [40, 41]. On the other hand, the dilepton measurements at RHIC are still in their infancy (first data indicate substantial excess radiation [42]), but it will become a central component in future runs [43]. Very interesting results are also emerging from vector-meson spectroscopy in cold nuclei using elementary projectiles, i.e., photons [44, 45] or protons [46]. It turns out that all of these observables are closely related, and their broad understanding is essential for the determination of the in-medium vector-meson spectral functions. Of particular importance is the consistency of theoretical descriptions beyond phenomenological applications and the interrelations between different approaches (including effective hadronic and quark models, lattice QCD and constraints from sum rules), which will ultimately reveal the mechanisms of chiral restoration. In this article, we give an up-to-date account of these efforts with special emphasis on a broader picture in the context of χSR.

1.4 Outline

Our article is organized as follows. In Sec. 2, we start by recollecting basic features of spontaneous chiral symmetry breaking in the QCD vacuum with emphasis on condensate structures and consequences for the hadronic excitation spectrum (sub-Sec. 2.1), followed by a discussion of in-medium condensates within the landscape of the QCD phase diagram (sub-Sec. 2.2). In Sec. 3, we scrutinize the links of the chain with which one hopes to connect thermal dilepton rates and (partial) χSR. We first introduce the EM correlation function which is the basic quantity figuring into the thermal dilepton rate (sub-Sec. 3.1). Model-independent evaluations of medium effects can be obtained in the low-density limit from current algebra, in the high-temperature limit from perturbative QCD and, for vanishing baryon-chemical potential from lattice QCD (sub-Sec. 3.2). A valuable source of model-independent constraints is provided by chiral and QCD sum rules (sub-Sec. 3.3) which are energy moments of spectral functions that directly relate to order parameters of QCD and are generally not restricted in temperature and density. For practical applications, effective hadronic models are an indispensable tool (sub-Sec. 3.4); their reliability, based on the choice of interaction vertices and associated parameters, crucially hinges

on a thorough procedure of theoretical and phenomenological constraints; an important question will also be the fate of the vector dominance model in the medium. In Sec. 4 the theoretical developments are tested in recent dilepton production experiments, starting with elementary reactions off nuclei representative for medium effects in cold nuclear matter (sub-Sec. 4.1). The main part of Sec. 4 is devoted to an analysis of dilepton spectra in ultrarelativistic heavy-ion reactions (sub-Sec. 4.2), focusing on recent results obtained at the CERN-SPS by the NA60 and CERES/NA45 collaborations. The spectral analysis is completed by a critical assessment of the combined theoretical and experimental status to date (sub-Sec. 4.3). We finish with concluding remarks in Sec. 5.

2 Chiral Symmetry, Condensates and Chiral Restoration

It is generally accepted that strong interactions are described by Quantum Chromodynamics (QCD), introduced in 1973 [47, 48, 49], with a Lagrangian density given by

$$\mathcal{L}_{QCD} = \bar{q}(i\gamma^\mu D_\mu - \mathcal{M}_q)q - \frac{1}{4}G^a_{\mu\nu}G^{\mu\nu}_a \quad , \qquad D_\mu = \partial_\mu + ig_s\frac{\lambda_a}{2}A^a_\mu \ , \tag{1}$$

formulated in terms of elementary quark (q) and gluon (A^a_μ) fields (γ^μ and λ^a: Dirac and Gell-Mann matrices, respectively, $\mathcal{M}_q$=diag$(m_u, m_d, \dots)$: current-quark mass matrix). In addition to the local $SU(3)$ color gauge symmetry, $\mathcal{L}_{QCD}$ possesses several global symmetries. The most relevant one in the present context is Chiral Symmetry, which can be exhibited by rewriting $\mathcal{L}_{QCD}$ in terms of left- and right-handed quark fields, $q_{L,R}=\frac{1}{2}(1\mp\gamma_5)q$:

$$\mathcal{L}_{\rm QCD} = \bar{q}_L i\gamma^\mu D_\mu q_L + \bar{q}_R i\gamma^\mu D_\mu q_R - (\bar{q}_L\mathcal{M}_q q_R + \bar{q}_R\mathcal{M}_q q_L) - \frac{1}{4}G^a_{\mu\nu}G^{\mu\nu}_a \ . \tag{2}$$

For small quark masses, i.e., u and d quarks, $\mathcal{L}_{\rm QCD}$ is approximately invariant under rotations $q_{L,R} \to {\rm e}^{-i\vec{\alpha}_{L,R}\cdot\vec{\tau}/2}q_{L,R}$, where $\vec{\alpha}_{R,L}$ are 3 real angles and τ operates in (u-d) isospin space. Chiral invariance of the QCD Lagrangian thus refers to the conservation of quark handed-ness and isospin. Alternatively, one can rewrite the chiral rotations as $q \to {\rm e}^{-i\vec{\alpha}_V\cdot\vec{\tau}/2}q$ and $q \to {\rm e}^{-i\gamma_5\vec{\alpha}_A\cdot\vec{\tau}/2}q$, giving rise to conserved isovector-vector and -axialvector currents,

$$\vec{j}^\mu_V = \bar{q}\gamma^\mu\frac{\vec{\tau}}{2}q \quad , \quad \vec{j}^\mu_A = \bar{q}\gamma^\mu\gamma_5\frac{\vec{\tau}}{2}q \ . \tag{3}$$

2.1 Condensates and Hadron Spectrum in Vacuum

As emphasized in the Introduction, the nonperturbative structure of the QCD vacuum is characterized by its condensates. A special role is played by the quark-antiquark ($q\bar{q}$) and gluon (G^2) condensates. Apart from being the condensates involving the minimal number of quark- and gluon-fields, the former is a main order parameter of SBχS while the latter dominantly figures into the energy-momentum tensor of the theory. The vacuum expectation value of the latter's trace is given by

$$\langle T^\mu_\mu\rangle = \epsilon - 3P = -\langle G^2\rangle + m_q\langle\bar{q}q\rangle \tag{4}$$

where $G^2 = -(\beta(g_s)/2g_s)\,G^{\mu\nu}_a G^a_{\mu\nu}$ involves the gluon-field strength tensor and the renormalization-group beta function, $\beta(g_s)$. The latter appears because the nonvanishing vacuum

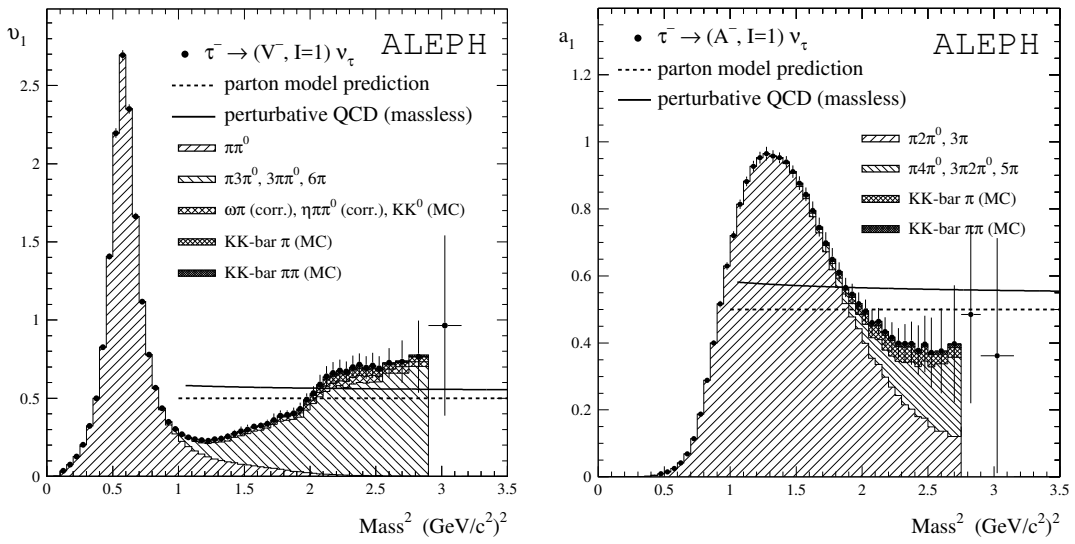

Figure 2: *Experimental data [50] of the isovector-vector (IJ^P=11^-, left panel) and isovector-axialvector (IJ^P=11^+, right panel) spectral functions from hadronic decays of τ leptons (produced in $\sqrt{s}$=91 GeV e^+e^- annihilation at LEP) into even and odd numbers of pions/kaons, respectively. The lines indicate theoretical calculations using pQCD.*

value of T^μ_μ breaks the scale invariance of the classical QCD Lagrangian, induced by quantum loop corrections. The small current light-quark masses, $m_q \simeq 5\,\mathrm{MeV}$, render the contribution of the quark condensate to T^μ_μ small. The absolute value of the gluon condensate is not precisely known, but presumably rather large, around $1.5\,\mathrm{GeV/fm^3} \simeq (330\,\mathrm{MeV})^4$. In fact, the magnitude of the quark condensate is not small either, $\langle\bar{q}q\rangle \simeq (\text{-}250\,\mathrm{MeV})^3$ per light-quark flavor, and about 50% of that for strange quarks. This implies that the vacuum is filled with $\sim$5 quark-antiquark pairs per fm^3! Also note that the quark condensate maximally violates chiral symmetry by mixing right- and left-handed quarks, $\langle\bar{q}q\rangle = \langle\bar{q}_L q_R + \bar{q}_R q_L\rangle$, implying that a quark propagating through the vacuum can flip its chirality by coupling to the condensate. The intimate relation between chiral symmetry breaking and the associated Goldstone-boson nature of the pion is highlighted by the Gell-Mann-Oakes Renner (GOR) relation,

$$m_\pi^2 f_\pi^2 = -2 m_q \langle\bar{q}q\rangle \ , \tag{5}$$

which combines the effects of explicit chiral symmetry breaking, $m_\pi^2 \propto m_q$, and SBχS with the pion decay constant as order parameter.

One of the best direct empirical evidences for the spontaneous breaking of chiral symmetry is found in the vector channel, more specifically the isovector-vector channel (IJ^P=11^+) and its chiral partner, the isovector-axialvector one (IJ^P=11^-), precisely the Noether currents in Eqs. (3). The pertinent spectral functions have been measured with excellent precision (and a detailed decomposition of the hadronic final states) at the Large Electron-Positron collider (LEP) in hadronic τ decays by the ALEPH [50] and OPAL [51] collaborations, cf. Fig. 2. In the low-mass region, the strength of each of the two spectral functions is largely concentrated in a prominent resonance, i.e., the $\rho(770)$ and $a_1(1260)$. This very fact indicates that the low-mass regime is dominated by nonperturbative effects, while the (large) difference in mass and width of these resonances signals chiral

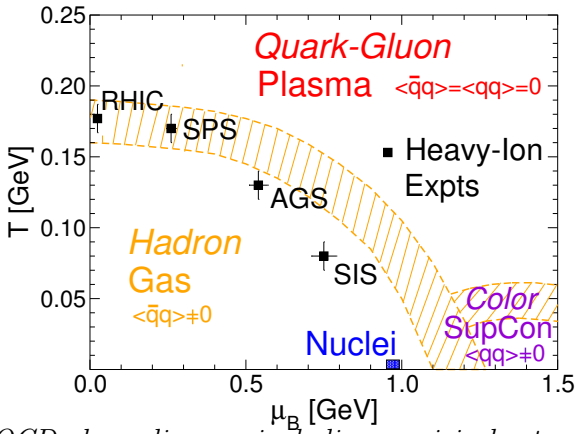

Figure 3: *Schematic QCD phase diagram including empirical extractions of* (μ_B, T)*-values from observed hadron production ratios in heavy-ion experiments at different beam energies [8]; the bands indicate lattice-QCD and model estimates of the transition regions between HM, QGP and CSC; with the HM-QGP transition (along the finite* T*,* μ_B*=0 axis) presumably a cross-over, and the HM-CSC one (along the finite* μ_B*,* T*=0 axis) possibly first order, there is presumably a second order endpoint, e.g., around* $(\mu_B, T)\approx$*(400,160) MeV.*

symmetry breaking. This connection can be quantified by chiral sum rules developed by Weinberg [52] and others [53] in the late 1960's based on current algebra of chiral symmetry. These sum rules relate moments of the difference between vector and axialvector spectral functions to chiral order parameters. In the chiral limit (m_π=0) one has

$$f_n = -\int_0^\infty \frac{\mathrm{d}s}{\pi}\, s^n \, \left[\mathrm{Im}\,\Pi_V(s) - \mathrm{Im}\,\Pi_A(s)\right] \ , \tag{6}$$

$$f_{-2} = f_\pi^2 \frac{\langle r_\pi^2\rangle}{3} - F_A \ , \quad f_{-1} = f_\pi^2 \ , \quad f_0 = 0 \ , \quad f_1 = -2\pi\alpha_s\langle\mathcal{O}\rangle \tag{7}$$

(r_π: pion charge radius, F_A: coupling constant for the radiative pion decay, $\pi^\pm \to \mu^\pm\nu_\mu\gamma$, $\langle\mathcal{O}_\triangle\rangle$: four-quark condensate).

2.2 Phase Diagram and Chiral Restoration

A schematic view of the QCD phase diagram is displayed in Fig. 3. It is roughly characterized by three major regimes (all of which most likely exhibit rich substructures): hadronic matter (HM) at small and moderate temperature (T) and baryon chemical potential (μ_B), Quark-Gluon Plasma (QGP) at high T and Color Super-Conductors (CSCs) at high μ_B but low T. The latter may occur in the core of neutron stars, but are unlikely to be produced in heavy-ion collisions and will not be further discussed here.

A key issue toward understanding the phase structure of QCD matter is the temperature and density dependence of its condensates. Various condensates serve as order parameters of broken symmetries and govern the (hadronic) excitation spectrum. The latter provides the connections to observables. A first estimate of the medium modifications of the condensates can be obtained in the low-density limit [55, 56], by approximating the thermal medium by non-interacting light hadrons, i.e., pions at finite T an nucleons at

finite ϱ_N. For the quark condensate, this leads to a linear density expansion of the type

$$\frac{\langle\!\langle\bar{q}q\rangle\!\rangle(T,\mu_B)}{\langle\bar{q}q\rangle} \;=\; 1-\sum_h \frac{\varrho_h^s\Sigma_h}{m_\pi^2 f_\pi^2} \;\simeq\; 1-\frac{T^2}{8f_\pi^2}-\frac{1}{3}\frac{\varrho_N}{\varrho_0}-\cdots \;, \tag{8}$$

where ρ_h^s denotes the scalar density of hadron h, and Σ_h denotes its "σ"-term (Σ_h/m_q may be interpreted as the number of $\bar{q}q$ pairs inside hadron h which diminish the (negative) $\bar{q}q$ density of the condensate). In obtaining Eq. (8), the GOR relation (5) has been used. Alternatively, one can directly use the definition of the quark condensate in terms of the quark-mass derivative of the thermodynamic potential,

$$\langle\!\langle\bar{q}q\rangle\!\rangle = \frac{\partial\Omega}{\partial m_q} \;, \tag{9}$$

and evaluate the temperature and density-dependent part, $\bar{\Omega}(\mu_B,T)\equiv\Omega(\mu_B,T)-\Omega_{\rm vac}$, in the free gas approximation. A similar strategy can be adopted for the gluon condensate, by utilizing its relation, Eq. (4), to the trace anomaly,

$$\langle\!\langle G^2\rangle\!\rangle = -(\epsilon-3P)+m_q\langle\!\langle\bar{q}q\rangle\!\rangle \;, \tag{10}$$

and estimating the ϱ_B- and T-dependent parts of pressure and energy density in suitable expansions. At finite temperature, for a massless pion gas, one has ϵ=$3P$ and thus no correction to order T^4 (the system is scale invariant). It turns out that the lowest-order interaction contribution from (soft) $\pi\pi$ scattering does not contribute either so that the leading temperature dependence of the gluon condensate arises at order T^8 [54]. With the leading nuclear-density dependence as worked out in Refs. [55, 56], one has

$$\langle\!\langle G^2\rangle\!\rangle = -\langle G^2\rangle-(m_N-\Sigma_N)\varrho_N-\frac{\pi^2}{270}\frac{T^8}{f_\pi^4}\left(\ln\frac{\Lambda_p}{T}-\frac{1}{4}\right) \tag{11}$$

($\Lambda_p$$\simeq$275 MeV is a renormalization scale). The above relations allow for some interesting insights. As already noted in Ref. [56], the linear-density expansions suggest that the gluon condensate is much less affected then the quark condensate, cf. also the upper panels in Fig. 4. It is not obvious whether recent finite-T lattice computations in QCD with 2+1 flavors support this picture (see the lower panels of Fig. 4), especially when approaching the critical temperature: both $\langle\!\langle\bar{q}q\rangle\!\rangle$ and $\langle\!\langle G^2\rangle\!\rangle$ drop significantly around T_c and reach approximately zero at roughly $1.5\,T_c$ (the perturbative interaction contribution to $\epsilon-3P$ renders the gluon condensate negative at high T). The low-density expansion of the quark condensate seems to suggest that temperature effects are weaker than density effects (upper left panel in Fig. 4). This is, in fact, not the case: as a function of (pion-) *density*, the leading reduction of $\langle\!\langle\bar{q}q\rangle\!\rangle$ in a heat bath is quite comparable to cold nuclear matter, as determined by the coefficient in Eq. (8) which is in essence given by the respective σ terms, $\Sigma_\pi$$\simeq$70 MeV compared to Σ_N=45$\pm$15 MeV.

Another interesting observation can be made when taking the expectation value of the trace of the energy momentum tensor over a single nucleon state,

$$\langle N|T^\mu_\mu|N\rangle = -m_N = \langle N|G^2|N\rangle + m_q\,\langle N|\bar{q}q|N\rangle \;. \tag{12}$$

Since the second term (related to the σ term) is small (or zero in the chiral limit), this relation seems to suggest that the major part of the nucleon mass is generated by the gluon condensate. This is to be contrasted with effective quark models (e.g., Nambu

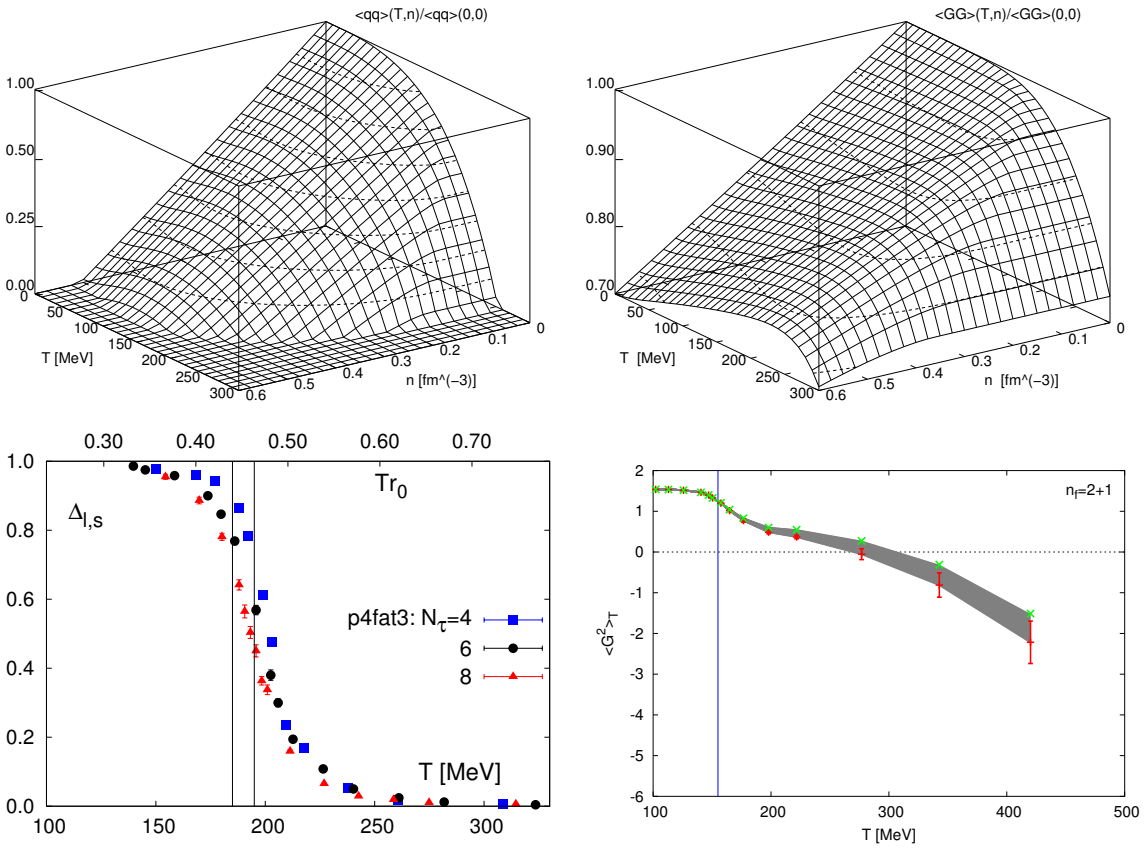

Figure 4: *Upper panels: density and temperature dependence of the chiral (left) and the gluon condensate (right), normalized to their vacuum values [57], obtained in a low-T and -ϱ_N expansions. Lower panels: T dependence at μ_q=0 of the (subtracted and renormalized) chiral condensate (left) [58] and of the gluon condensate (right) [59] as obtained from N_f=2+1 lattice QCD computations.*

Jona-Lasinio) which, in mean field approximation, attribute the constituent quark mass entirely to the quark condensate, m_q^*=$G_{\rm eff}\langle\bar{q}q\rangle$. One should also note that, at least in the QGP phase, the vanishing of the quark or gluon condensate does not necessarily imply quark "masses" to vanish. E.g., in perturbative QCD, partons in the QGP acquire a thermal mass $m_{q,g}^{\rm th}\sim gT$. This mass term does not break chiral symmetry (its Dirac structure includes a γ_0 matrix) and presumably persists until close to T_c, thus supplanting the constituent quark mass, m_q^*, well before the latter vanishes. This has, of course, important consequences for the masses of hadronic states in the vicinity of T_c. In addition, large binding-energy effects can be present, e.g., for the pion: if the chiral transition is continuous, the pion's Goldstone-boson nature could very well imply that it survives as a bound state at temperatures above T_c [60, 61, 62].

As emphasized above, the only known direct way to extract observable consequences of changes in the QCD condensate structure is to probe medium modifications in its excitation spectrum. This applies in particular for the quark condensate which has a rather small impact on the bulk properties of QCD matter being suppressed by m_q (the relation of the gluon condensate to the equation of state could, in principle, be tested via hydrodynamic or transport properties, but this turned out to be difficult in the context

of heavy-ion collisions [10]). The generic model-independent consequence of χSR for the in-medium hadronic spectrum is the degeneracy of the spectral functions within chiral multiplets (i.e., for chiral partners) , e.g., π-"σ", N-$N^*(1535)$ and $\rho(770)$-$a_1(1260)$. In the "σ" channel (which asymptotically corresponds to a scalar-isoscalar pion pair), interesting medium effects have been observed in pion- and photon-induced production of S-wave pion pairs off nuclei [63, 64, 65]. An accumulation of strength close to the two-pion threshold (which is not observed in the isotensor π-π channel) has been associated with an in-medium reduction of the "σ"-meson mass as a precursor effect of χSR [66] (note that the leading-density approximation, Eq. (8), predicts a reduction of the quark condensate by $\sim$30% already at normal nuclear matter density). However, nuclear many-body effects [67, 68], in particular the renormalization of the pion propagator in the nuclear medium, can essentially explain the experimental findings[4]. This raises an important question: to what extent do "conventional" in-medium effects encode mechanisms of χSR? From the point of view of the "σ" spectral function alone, it is not possible to distinguish whether a softening is caused by many-body effects or genuine mass changes figuring via medium modifications of the mass parameter in the underlying effective Lagrangian. Thus, a distinction of medium effects into "conventional" ones and those associated with an apparent "direct" connection to χSR is meaningless. Rather, a careful and exhaustive treatment of hadronic many-body effects is an inevitable ingredient for evaluating mechanisms of χSR. As already alluded to in the Introduction, a practical problem of using the $\pi\pi$ decay channel for studying medium effects are the strong final-state interactions of the individual pions when exiting the nuclear medium [69]. The same applies to the heavy-ion collision environment, implying that the $\pi\pi$ channel can only probe the dilute stages of the produced medium. This problem is overcome by dilepton final states, on which we will focus in the following.

3 Vector Mesons in Medium

3.1 Dileptons and Electromagnetic Correlation Function

For a strongly interacting medium in thermal equilibrium the production rate of dileptons can be cast into the form [16, 18],

$$\frac{dN_{ll}}{d^4x d^4q} = -\frac{\alpha_{\rm em}^2}{\pi^3 M^2}\; f^B(q_0;T)\; \frac{1}{3}\; g_{\mu\nu}\; \mathrm{Im}\,\Pi_{\rm em}^{\mu\nu}(M,q;\mu_B,T)\;. \tag{13}$$

This expression is to leading order in the electromagnetic (EM) coupling constant, $\alpha_{\rm em}$, but exact in the strong interaction. The latter is encoded in the EM spectral function, defined via the retarded correlator of the hadronic EM current, $j_{\rm em}^\mu(x)$,

$$\Pi_{\rm em}^{\mu\nu}(q_0,q)) = -\mathrm{i}\int d^4x\; e^{iq\cdot x}\; \Theta(x_0)\; \langle\!\langle [j_{\rm em}^\mu(x), j_{\rm em}^\nu(0)] \rangle\!\rangle\;. \tag{14}$$

In the vacuum, the spectral strength is directly accessible via the total cross section for e^+e^- annihilation,

$$\sigma(e^+e^- \to \text{hadrons}) = \frac{4\pi\alpha_{\rm em}^2}{s}\;\frac{(-12\pi)}{s}\,\mathrm{Im}\,\Pi_{\rm em}^{\rm vac}(s)\;, \tag{15}$$

recall Fig. 1 (the first factor is simply $\sigma(e^+e^-\to\mu^+\mu^-)=4\pi\alpha_{\rm em}^2/s$). As a function of invariant dilepton mass, $M^2=q_0^2-\vec{q}^2$, the spectrum basically decomposes into two regimes. In

[4]Similar results are obtained from a transport treatment of pion reinteractions in the medium [69].

the low-mass region (LMR, $M\leq$1 GeV), the strength is absorbed in the three vector mesons $\rho(770)$, $\omega(782)$ and $\phi(1020)$ representing the lowest resonances in the two-pion, three-pion and kaon-antikaon channels, respectively. Thus, the EM current is well described within the vector dominance model (VDM) [19] as given by the field current identity,

$$j^\mu_{\rm em}(M \leq 1 \text{ GeV}) = \frac{m_\rho^2}{g_\rho}\rho^\mu + \frac{m_\omega^2}{g_\omega}\omega^\mu + \frac{m_\phi^2}{g_\phi}\phi^\mu \,. \tag{16}$$

In the intermediate mass region (IMR, 1 GeV$<M\leq$3 GeV), the strength is reasonably well accounted for by a partonic description,

$$j^\mu_{\rm em}(M > 1.5 \text{ GeV}) = \sum_{q=u,d,s} e_q \; \bar{q}\gamma^\mu q \;, \tag{17}$$

where e_q denotes the electric quark charge in units of the electron charge, e. The connection between the two representations can be exhibited by rearranging the charge-flavor content of the quark basis into hadronic isospin quantum numbers,

$$j^\mu_{\rm em} = \frac{1}{\sqrt{2}}\left[\frac{\bar{u}\gamma^\mu u - \bar{d}\gamma^\mu d}{\sqrt{2}} + \frac{1}{3}\frac{\bar{u}\gamma^\mu u + \bar{d}\gamma^\mu d}{\sqrt{2}} - \frac{\sqrt{2}}{3}\bar{s}\gamma^\mu s\right] \;, \tag{18}$$

reflecting the quark content of the (normalized) ρ (isospin I=1), ω (I=0) and ϕ (I=0) wave functions, respectively. Converting the isospin coefficients into numerical weights in the EM spectral function, one obtains

$$\text{Im}\,\Pi_{\rm em} \sim \left[\text{Im}\,D_\rho + \frac{1}{9}\,\text{Im}\,D_\omega + \frac{2}{9}\,\text{Im}\,D_\phi\right] \;, \tag{19}$$

which identifies the isovector (ρ) channel as the dominant source (experimentally it is even larger as given by the electromagnetic decay widths, $\Gamma_{\rho\to ee}/\Gamma_{\omega\to ee}\simeq$ 11). Explicitly evaluating the EM correlators using the currents (16) and (17) yields

$$\text{Im}\,\Pi^{\rm vac}_{\rm em}(M) = \begin{cases} \sum\limits_{V=\rho,\omega,\phi}\left(\frac{m_V^2}{g_V}\right)^2 \text{Im}\,D_V^{\rm vac}(M) & ,\; M < M_{\rm dual}^{\rm vac}, \\ -\frac{M^2}{12\pi}\,(1+\frac{\alpha_s(M)}{\pi}+\dots)\,N_c\sum\limits_{q=u,d,s}(e_q)^2 & ,\; M > M_{\rm dual}^{\rm vac} \end{cases} \tag{20}$$

($M_{\rm dual}^{\rm vac}\simeq$ 1.5 GeV, N_c=3: number of quark colors, $D_V = 1/[M^2 - m_V^2 - \Sigma_V]$: vector-meson propagators). The associated processes in the thermal dilepton *production* rates are, of course, the inverse of e^+e^- annihilation, i.e., two-pion, three-pion and $K\bar{K}$ annihilation (channeled through the ρ, ω and ϕ) in a hadronic phase[5] and $q\bar{q}$ annihilation in a QGP. But what about hadronic emission in the IMR and QGP emission in the LMR? The former follows from time-reversal invariance of strong interactions: to the extent that the hadronic final state in e^+e^- annihilation can be represented by a statistical (thermal) distribution (which is empirically approximately satisfied), hadron-gas emission in the IMR corresponds to multi-hadron annihilation ($4\pi, 6\pi \to e^+e^-$, etc., which may be built from 2ρ, πa_1, $\pi\omega$, etc.), with a total strength given by the partonic continuum. QGP emission in the LMR is, of course, closely related to a central question of this review: How

[5]Note that the dominance of the isovector channel is naturally associated with the annihilation of the two lightest constituents in a hadronic medium.

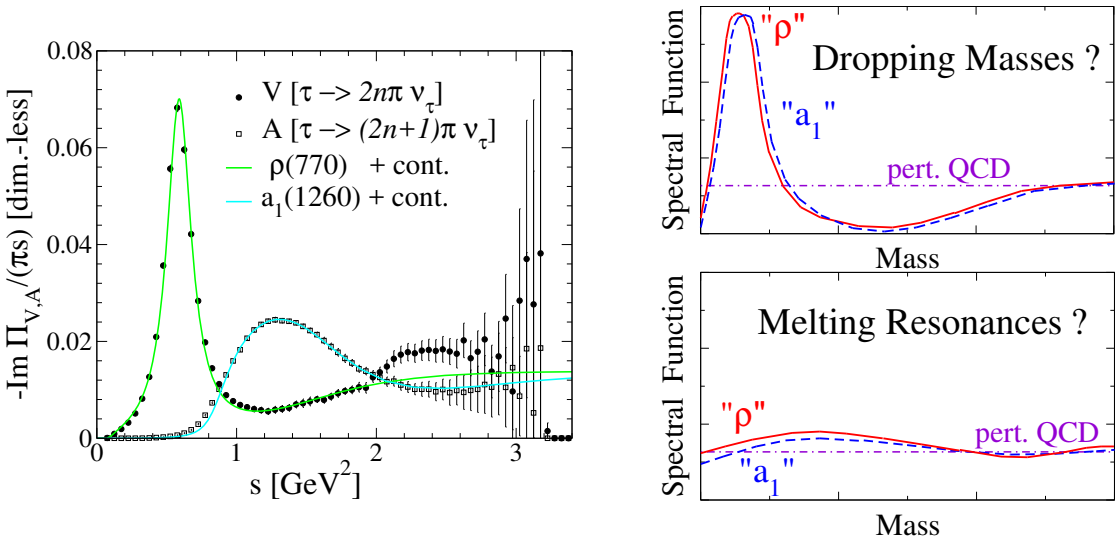

Figure 5: *Left panel: vector and axialvector spectral functions as measured in hadronic τ decays [50] with model fits using vacuum ρ and a_1 strength functions supplemented by perturbative continua [70]; right panel: scenarios for the effects of chiral symmetry restoration on the in-medium vector- and axial-vector spectral functions.*

does the dilute hadronic resonance gas rate evolve into the chirally restored, deconfined QGP rate? At sufficiently low temperatures and/or baryon densities virial expansions in a hadronic basis can provide initial insights. With increasing T and ϱ_B resummations become necessary for which many-body approaches are a suitable tool. It is currently an open question how far up in ϱ_B and T these calculations are reliable. Selfconsistent schemes are, in principle, capable of describing phase-transition dynamics, which, ideally, could be constrained by unquenched lattice-QCD calculations of the dilepton rate below T_c (energy sum rules turn out to be particularly useful to connect spectral functions to order parameters). Eventually, in the high-temperature limit, the LMR rate should recover perturbative $q\bar{q}$ annihilation, where a systematic evaluation of corrections becomes feasible again. The remainder of this section is devoted to a discussion of these approaches. With hindsight to Sec. 4, we will focus on models for which quantitative applications to dilepton observables have been made, with the isovector (ρ) channel playing the leading role. In the following, for brevity, we refer to the IJ^P=$11^{\pm}$ chiral partner channels as vector (V) and axialvector (A) ones. In the vacuum, both can be well represented by a low-lying resonance pole (ρ and a_1) and a continuum above, see left panel of Fig. 5. Two schematic scenarios for the degeneration of vector and axialvector channels at chiral restoration ("dropping mass" and "resonance melting") are sketched in the right panel of Fig. 5.

3.2 Medium Effects I: Model Independent

In principle, model-independent assessments of medium effects do not involve free parameters. These can be realized by virial expansion schemes based on experimental input for vacuum spectral functions (valid for dilute hadronic matter), perturbative QCD calculations (valid in the high-T limit) or first-principle lattice QCD computations.

3.2.1 Chiral Reduction and Mixing

The leading temperature dependence of vector and axialvector correlators, $\Pi^{\mu\nu}_{V,A}$, i.e., their modification in a dilute pion gas, can be inferred from chiral reduction and current algebra. They allow to simplify 1-pion matrix elements of any operator according to

$$\langle 0|\mathcal{O}|\pi^a\rangle = -\frac{i}{f_\pi}\langle 0|[Q_A^a,\mathcal{O}]|0\rangle \quad , \qquad [Q_A^a, j_{V,A}^{\mu,b}] = i\epsilon^{abc} j_{A,V}^{\mu,c} \ , \tag{21}$$

where $\{a,b,c\}$ are isospin indices. Evaluating the Fourier transforms of the thermal expectation values in the chiral and soft pion limit (i.e., m_π=0 and neglecting any momentum transfer k from thermal pions in the heat bath), one obtains the "mixing" theorem [71]

$$\Pi_{V,A}(q) = (1-\varepsilon)\ \Pi^0_{V,A}(q) + \varepsilon\ \Pi^0_{A,V}(q) \tag{22}$$

with the mixing parameter ε=$T^2/6f_\pi^2$ (the Lorentz structure remains as in the vacuum). The leading-T effect on the V and A correlators is a mere admixture of the chiral partner with a corresponding reduction of its original strength, via processes of the type $\pi+V \leftrightarrow A$ and $\pi + A \leftrightarrow V$; width and mass of the vacuum correlators are unaffected. For dilepton production, this implies a reduced ρ pole strength as well as an enhancement of the "dip" region, $M\simeq$1-1.5 GeV, where the a_1 resonance provides a "maximal feeding".

When naively extrapolating the mixing expression, Eq. (22), to chiral restoration (ε=1/2), one finds T_c=$\sqrt{3}f_\pi$=160 MeV. This is, however, misleading for several reasons. First, this estimate does not coincide with a similar extrapolation for the vanishing of the chiral condensate, cf. Eq. (8). Second, even a moderate amendment in terms of a finite pion mass in the scalar density shifts the estimate to $T_c\simeq$225 MeV. Both facts underline the inadequacy of the extrapolation of a lowest-order result. Third, the chiral and soft-pion limits are kinematically not a good approximation (e.g., at T=150 MeV, thermal pions typically bring in an energy of ∼300-400 MeV). In cold nuclear matter, a similar mixing is operative via the coupling of the pion cloud of ρ and a_1 to the nuclear medium [72, 73].

A much more elaborate treatment of the chiral reduction formalism has been conducted in Refs. [74, 75, 76]. These calculations are based on realistic fits to vacuum correlators, do not invoke kinematic approximations (chiral or soft-pion limits) and include both pion and nucleon ensembles. The leading-density part has been subjected to constraints from nuclear photo-absorption including the first and second resonance region via $\Delta(1232)$ and $N(1520)$ excitations. This allows for meaningful applications to dilepton spectra which have been carried out and will be discussed in Sec. 4. Note that these calculations do not explicitly invoke the notion of VDM, but the fact that the vacuum correlators are constructed with ρ and a_1 pole dominance, which is not upset in the linear density scheme, implies that VDM is still present upon inclusion of medium effects.

3.2.2 Lattice QCD and Susceptibilities

First-principle computations of light-hadron correlation functions in medium are based on a lattice discretized form of the finite-T QCD partition function. Besides a finite lattice spacing, additional approximations currently involve the restriction to finite volumes as well as the use of unphysically large up- and down-quark masses in the simulations. Furthermore, the implementation of chiral symmetry is not trivial in the lattice formulation. The numerical evaluation of the QCD path integral, is facilitated by transforming the action to imaginary (Euclidean) time, which converts the oscillatory behavior of the

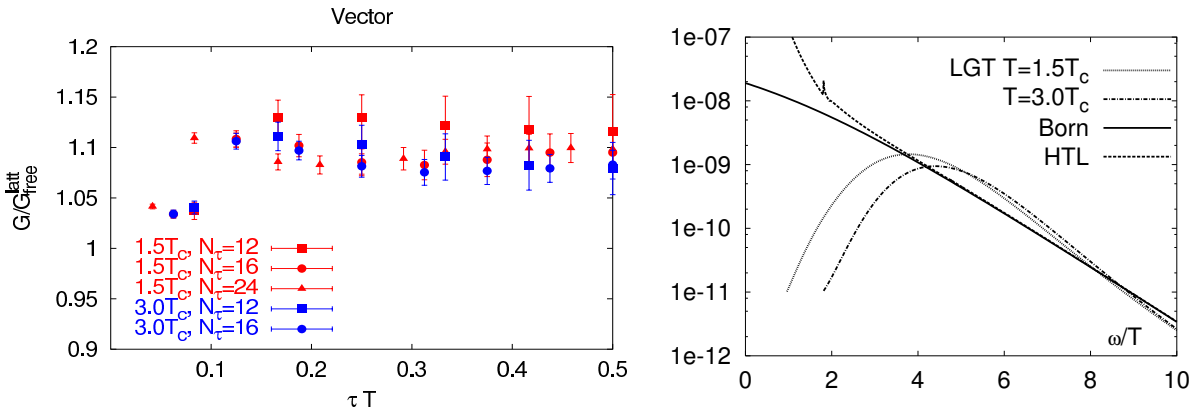

Figure 6: *Left panel: vector correlation function as a function of Euclidean time as evaluated in quenched lattice QCD for a gluon plasma at temperatures above T_c [77]. The in-medium correlators are normalized to the free one using the integration Kernel at the same temperature (the so-called "reconstructed" correlator). Right panel: thermal dilepton rates, $dN/(d^4qd^4x)$, in quenched lattice QCD as extracted from the correlation functions shown in the left panel using the maximum entropy method. The lattice results are compared to calculations in perturbation theory, either to leading order ($\mathcal{O}(\alpha_s^0)$) $q\bar{q}$ annihilation (solid line) or within the hard-thermal-loop (HTL) framework [78] (dashed line). All rates are calculated at a total pair 3-momentum of q=0, i.e., the dilepton energy, ω=q_0, equals its invariant mass, M.*

integrand in the partition function into an exponential damping. The pertinent Euclidean correlation function, $\Pi(\tau)$, is related to the physical spectral function, $\rho = -2\,\mathrm{Im}\,\Pi$, via

$$\Pi(\tau, q; T) = \int_0^\infty \frac{dq_0}{2\pi}\, \rho(q_0, q; T)\, \frac{\cosh[(q_0(\tau - 1/2T)]}{\sinh[q_0/2T]}\ . \tag{23}$$

The resulting Euclidean vector correlators in "quenched" QCD[6] above T_c shows a moderate enhancement over the free correlator, cf. left panel of Fig. 6 [77]. The extraction of the spectral function requires an inverse integral transform over a finite number of τ points[7] which can only be achieved with a probabilistic treatment based on the "Maximum Entropy Method" [79]. The resulting strength function has been inserted into the dilepton rate and is compared to perturbative QCD (pQCD) rates in the right panel of Fig. 6. The leading-order pQCD corresponds to the $q\bar{q}$ strength distribution in Eq. (20), lower line, while the hard-thermal-loop (HTL) improved rate is from Ref. [78]. The latter shows the expected divergence for $M \to 0$ which is caused by the Bose factor and photon propagator which overcome the $\rho \propto q_0$ dependence of a retarded correlation function (cf. also Ref. [80]). This feature is not shared by the lattice result which might be an artifact of, e.g., the finite-volume restriction (it would also suggest a small or even vanishing photon production rate). On the other hand, the enhancement in the Euclidean correlator translates into an enhanced dilepton rate at energies of a few times the temperature. Whether this reflects a broad resonance structure is not clear at present.

[6] In the "quenched" approximation the fermionic part of the QCD action is neglected in the evaluation of the Euclidean path integral. This amounts to neglecting fermion loops.

[7] The (anti-) periodicity of the boson (fermion) fields at finite T restricts the Euclidean time direction to the interval $[0, \beta]$ where $\beta = 1/T$.

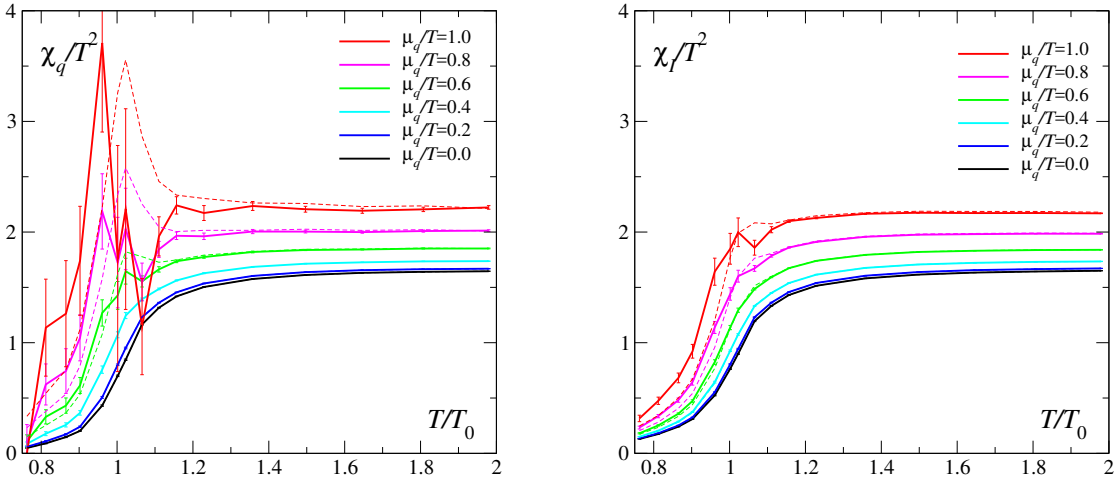

Figure 7: *Isoscalar (left) and isovector (right) quark-number susceptibility for various quark chemical potentials, $\mu_q = \mu_B/3$, as computed in unquenched lattice QCD [81].*

Additional constraints from lattice QCD are provided by susceptibilities which are defined as second-order derivatives of the thermodynamic potential. In our context, the quark-number susceptibilities are of special interest,

$$\chi_\alpha \sim \frac{\partial^2 \Omega}{\partial \mu_\alpha^2} \sim \Pi_\alpha(q_0 = 0, q \to 0) \ , \tag{24}$$

which can be decomposed in isoscalar ($\mu_q = (\mu_u + \mu_d)/2$) and isovector ($\mu_I = (\mu_u - \mu_d)/2$) channels carrying the quantum numbers of the ω and ρ, respectively. The spacelike limits of the correlators basically represent the screening masses in the respective channels. Lattice QCD computations of the quark-number susceptibilities indicate that both ρ and ω channels behave smoothly with temperature for small chemical potentials, see Fig. 7. However, as μ_q increases, χ_q develops a peak whereas χ_I remains smooth. The former indicates an increase in the (local) baryon-number fluctuations and may be a precursor of the baryon-number discontinuity between hadronic and QGP phase as one is approaching a first-order line. Remarkably, this is not seen for the isospin fluctuations.

3.3 Sum Rules and Order Parameters

Sum rules are currently the most promising tool to connect the nonperturbative physics encoded in spectral functions to the condensate structure of the QCD vacuum. In particular, the Weinberg sum rules directly relate order parameters of χSR to the axial-/vector spectral functions, which, in the medium, have not been exploited much to date.

3.3.1 Chiral Sum Rules

The Weinberg and DMO sum rules [52, 53], Eqs. (6), directly relate moments of the "vector minus axialvector" spectral functions to chiral order parameters. This is a rather fortunate situation in view of the dominant role that the isovector-vector (ρ) channel plays in dilepton production, recall Eq. (19). For N_f=2, the ω is a chiral singlet, while in the strangeness sector (ϕ), i.e., for N_f=3, chiral symmetry becomes much less accurate (e.g., $\langle\langle \bar{s}s \rangle\rangle$ persists much farther into the QGP).

As has been shown in Ref. [82], the Weinberg sum rules remain valid at finite temperature, albeit with two important modifications induced by the breaking of Lorentz invariance caused by the heat bath which defines a preferred rest frame: (i) each energy sum rule applies for a fixed three-momentum, and (ii) at finite three-momentum, the vector and axialvector spectral functions split into longitudinal and transverse modes,

$$\Pi_V^{\mu\nu} = \Pi_{V,A}^T P_T^{\mu\nu} + \Pi_{V,A}^L P_L^{\mu\nu} \ , \tag{25}$$

with individual sum rules for each of them. The explicit form is as follows:

$$-\int_0^\infty \frac{\mathrm{d}q_0^2}{\pi(q_0^2-q^2)} \left[\mathrm{Im}\,\Pi_V^L(q_0,q) - \mathrm{Im}\,\Pi_A^L(q_0,q)\right] \;=\; 0, \tag{26}$$

$$-\int_0^\infty \frac{\mathrm{d}q_0^2}{\pi} \left[\mathrm{Im}\,\Pi_V^{L,T}(q_0,q) - \mathrm{Im}\,\Pi_A^{L,T}(q_0,q)\right] \;=\; 0, \tag{27}$$

$$-\int_0^\infty q_0^2 \frac{\mathrm{d}q_0^2}{\pi} \left[\mathrm{Im}\,\Pi_V^{L,T}(q_0,q) - \mathrm{Im}\,\Pi_A^{L,T}(q_0,q)\right] \;=\; -2\pi\alpha_s \langle\langle \mathcal{O}_4 \rangle\rangle \ . \tag{28}$$

In writing Eqs. (26)-(28) the pionic piece of the (longitudinal) axialvector correlator has been absorbed into the definition of the in-medium spectral function, $\mathrm{Im}\,\Pi_A^L(q_0,q)$; in the vacuum and in the chiral limit it is represented by a sharp state, $\mathrm{Im}\,\Pi_\pi^{\mu\nu}=f_\pi^2 M^2\delta(M^2)P_L^{\mu\nu}$. In this form it only contributes to the first sum rule, Eq. (26). However, in matter (and for $m_\pi>0$) this is no longer true since the pion is expected to undergo substantial medium effects.

The in-medium chiral sum rules constitute a rich source of constraints on both energy and three-momentum dependence of in-medium spectral functions. The energy moments demonstrate that chiral restoration requires degeneracy of the entire spectral functions. Combining lQCD computations of order parameters with effective model calculations thus provides a promising synergy for deducing chiral restoration from experiment [43].

3.3.2 QCD Sum Rules

QCD sum rules are based on a (subtracted) dispersion relation for a correlation function in a given hadronic channel α, formulated for spacelike momenta $q^2=-Q^2<0$ [83],

$$\Pi_\alpha(Q^2) = \Pi_\alpha(0) + \Pi'_\alpha(0)\ Q^2 + Q^4 \int \frac{\mathrm{d}s}{\pi s^2} \frac{\mathrm{Im}\,\Pi_\alpha(s)}{s+Q^2} \ . \tag{29}$$

The right-hand-side (*rhs*) contains the spectral function which is usually related to observables or evaluated in model calculations. On the left-hand-side (*lhs*), the correlation function is expanded into a power series of $1/Q^2$ (operator-product expansion = OPE) where the (Wilson) coefficients contain perturbative contributions as well as vacuum-expectation values of quark and gluon operators (the nonperturbative condensates; for practical purposes the convergence of the OPE is improved by means of a so-called Borel transformation which we do not discuss here). The explicit form of the OPE for vector and axialvector correlators reads (truncating higher order terms in m_q, α_s, etc.)

$$\frac{\Pi_V^{\mathrm{vac}}}{Q^2} = -\frac{1+\frac{\alpha_s}{\pi}}{8\pi^2}\ln\frac{Q^2}{\mu^2} + \frac{m_q\langle\bar{q}q\rangle}{Q^4} + \frac{1}{24Q^4}\ \langle\frac{\alpha_s}{\pi}{G^a_{\mu\nu}}^2\rangle - \frac{112\pi\alpha_s}{81Q^6}\ \kappa\ \langle\bar{q}q\rangle^2 + \cdots \tag{30}$$

$$\frac{\Pi_A^{\mathrm{vac}}}{Q^2} = -\frac{1+\frac{\alpha_s}{\pi}}{8\pi^2}\ln\frac{Q^2}{\mu^2} - \frac{m_q\langle\bar{q}q\rangle}{Q^4} + \frac{1}{24Q^4}\ \langle\frac{\alpha_s}{\pi}{G^a_{\mu\nu}}^2\rangle + \frac{176\pi\alpha_s}{81Q^6}\ \tilde{\kappa}\ \langle\bar{q}q\rangle^2 + \cdots \tag{31}$$

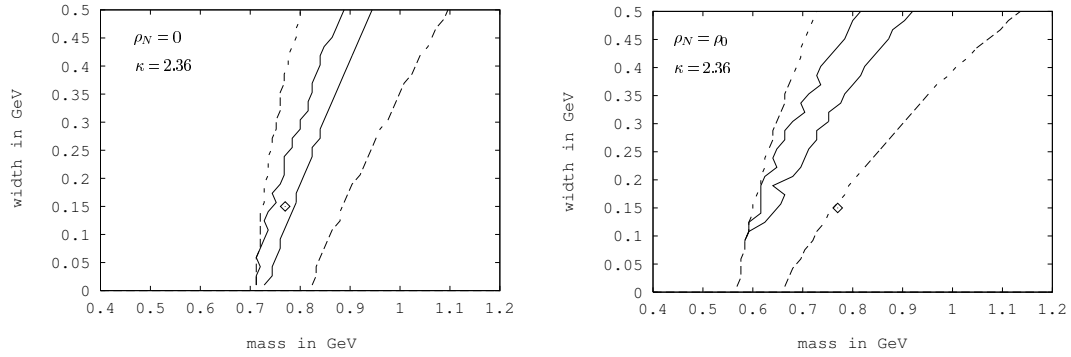

Figure 8: *QCD sum rule constraints on ρ meson mass and width as inferred from Breit-Wigner parameterizations of its spectral function [87] (left panel: vacuum, right panel: cold nuclear matter at saturation density). "Allowed" regions of mass and width are indicated by the bands between solid and dashed curves, corresponding to maximal deviations between the l.h.s and r.h.s. of the SR of 0.2% and 1%, respectively. The diamond depicts the corresponding vacuum parameters.*

where the four-quark condensates have been approximated by factorizing them into the squared two-quark condensate with parameters κ, $\tilde{\kappa}$ which simulate intermediate states other than the ground state (the scale μ is typically chosen around 1 GeV). Note that SBχS is nicely reflected by the opposite signs of the quark-condensate terms in Π_V and Π_A, while the "flavor-blind" gluon condensate enters with the same sign. Qualitatively, the (positive) gluon condensate actually induces a softening of the spectral function (i.e., a larger weight at small s in the dispersion integral) [84]. On the other hand, for the vector channel, the negative contributions from the quark condensates on the *lhs* of the sum rule push spectral-function strength to larger s, relative to the axialvector channel (this may seem surprising in view of the masses of the pertinent resonances, m_ρ=0.77 GeV vs. m_{a_1}=1.23 GeV; recall, however, that the (longitudinal) axialvector channel contains a contribution from the axialvector current of the pion). Inserting numerical values, α_s=0.35, m_q=0.005 GeV, $\langle\bar{q}q\rangle$=(-0.25 GeV)^3 and $\langle\frac{\alpha_s}{\pi}G^a_{\mu\nu}{}^2\rangle$=0.012 GeV^4, leads to

$$\frac{\Pi_V^{\rm vac}}{Q^2} = \frac{1}{8\pi^2}\left(-1.11\ln\frac{Q^2}{\mu^2} - \frac{0.0062\ {\rm GeV}^4}{Q^4} + \frac{0.039\ {\rm GeV}^4}{Q^4} - \frac{0.029\ {\rm GeV}^6\ \kappa}{Q^6}\right)\ , \quad (32)$$

illustrating that the leading contributions arise from the gluon and four-quark condensates (especially for typical values of $\kappa\simeq$2.5), while the impact of the quark condensate is rather moderate. For the vector channel, and in vacuum, there is a large cancellation between the gluon and 4-quark condensate terms. However, in the medium this is presumably lifted, especially at low T and ρ_B where quark and gluon condensates change rather differently. The stronger reduction of the "repulsive" 4-quark condensate relative to the "attractive" gluon condensate induces a softening of the spectral function in the dispersion integral. The softening can be satisfied by both broadening and/or a downward mass shift [85, 86, 87, 88, 89]. Quantitative studies (which also include effects of non-scalar condensates induced by hadron structure of the heat-bath particles) based on Breit-Wigner model spectral functions are displayed in Fig. 8. For the axialvector channel, the reduction in both condensates suggests a substantial loss of soft-mode strength which points at the dissolution of the pion mode (whose polestrength is given by f_π) as a consequence of (the approach toward) χSR.

Finally, it is instructive to compare ω and ρ mesons: while their OPE side is rather similar (governed by 4-quark condensates), the subtraction constant, $\Pi_V(0) = \varrho_N/4M_N$ to leading order in ϱ_N, makes a difference. It is given by the Thompson limit of the VN scattering amplitude and turns out to be identical in the ρ and ω sum rule. However, since Im Π_ρ is larger than Im Π_ω by an isospin factor of $(g_\omega/g_\rho)^2 \simeq 9$ (recall Eq. (19)), the finite-ϱ_N subtraction actually stabilizes the ω sum rule, implying stronger medium effects (softening) on the ρ than on the ω (it amounts to a "repulsive" contribution on the OPE side counterbalancing the reduction in the 4-quark condensate).

3.4 Medium Effects II: Chiral Effective Models

Model-independent and/or low-density approaches as discussed above provide valuable constraints on the vector and axialvector correlators and their connections to QCD vacuum structure. However, quantitative calculations suitable for comparison with experiment require the construction of effective models. As indicated in the Introduction, in the low-mass region most of the thermal dilepton yield in heavy-ion collisions is expected to emanate from the hot/dense hadronic phase (even at collider energies), especially from the ρ channel. Hadronic chiral Lagrangians are therefore a suitable starting point, extended by the implementation of the low-lying vector mesons. This is usually done by a local gauging procedure of the chiral pion Lagrangian, thus realizing the gauge principle at the composite (hadronic) level. The most common approaches are based on non-linear realizations of chiral symmetry (i.e., without explicit σ meson) within the Hidden Local Symmetry (HLS) [90] or Massive Yang Mills (MYM) [91] schemes. Rather than reviewing these in a comprehensive form, we here focus on recent developments with relevance for dilepton production, i.e., the "vector manifestation" (VM) scenario of SBχS within HLS [92] (Sec. 3.4.1), as well as hadronic many-body theory within MYM (Sec. 3.4.2).

3.4.1 Hidden Local Symmetry and Vector Manifestation

Within the HLS framework, an alternative realization of chiral symmetry in the meson spectrum has been suggested in Ref. [92], by identifying the chiral partner of the pion with the (longitudinal) ρ (rather than with the σ). This "vector manifestation" of chiral symmetry has been shown to give a satisfactory phenomenology of hadronic and EM decay branchings in the vacuum. When applied within a finite-T loop expansion, the ρ-meson mass was found to be affected at order T^4 (consistent with chiral symmetry), showing a slightly repulsive shift. However, when matching the hadronic axial-/vector correlators to pQCD in the spacelike regime (using an OPE), a reduction of the bare ρ mass has been inferred, consistent with "Brown-Rho" scaling [21]. In addition, vector dominance was found to be violated in the medium, leading to a gradual decoupling of the ρ from the EM current toward the critical temperature. However, the finite-T EM formfactor, which determines the dilepton production rate, clearly shows the downward moving ρ peak [93], see Fig. 9. An interesting question is how these features develop in the presence of finite baryon density.

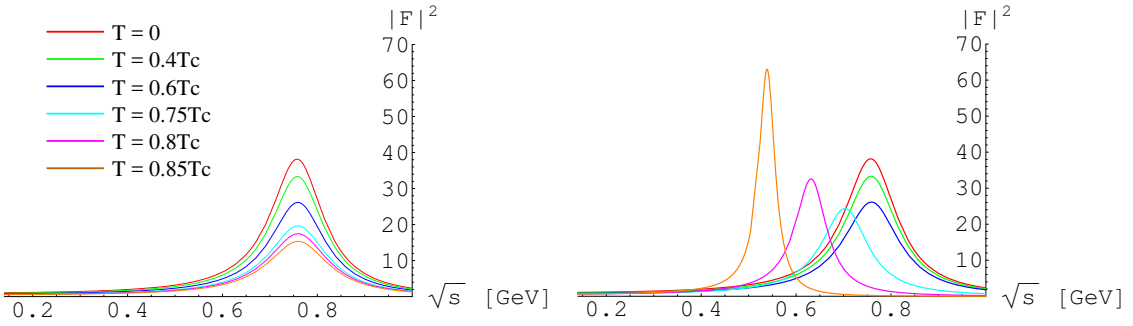

Figure 9: *Pion EM formfactor at finite temperature in the HLS vector manifestation framework [93]; left panel: with finite-T loop effects; right panel: additionally including a T-dependence of the bare ρ mass above $T{=}0.7T_c$.*

3.4.2 Massive Yang-Mills and Hadronic Many-Body Theory

As in HLS, the basic building block of the MYM Lagrangian is the chiral pion Lagrangian based on the unitary pion field,

$$U = \exp(i\sqrt{2}\phi/f_\pi) \ , \qquad \phi \equiv \phi_a \frac{\tau_a}{\sqrt{2}} \ . \tag{33}$$

Hadronic gauge fields, $A^\mu_{L,R}$ are introduced via the covariant derivative,

$$D^\mu U = \partial^\mu - ig(A^\mu_L U - U A^\mu_R) \tag{34}$$

and supplemented with kinetic and mass terms (with bare mass m_0). One has

$$\begin{aligned} \mathcal{L}_{\rm mym} \ &= \ \frac{1}{4}f_\pi^2 \ {\rm tr}\left[D_\mu U D^\mu U^\dagger\right] - \frac{1}{2}\,{\rm tr}\left[(F_L^{\mu\nu})^2 + (F_R^{\mu\nu})^2\right] + m_0^2 \ {\rm tr}\left[(A_L^\mu)^2 + (A_R^\mu)^2\right] \\ &\quad -i\xi \ {\rm tr}\left[D_\mu U D^\mu U^\dagger F_L^{\mu\nu} + D_\mu U D^\mu U^\dagger F_R^{\mu\nu}\right] + \sigma \ {\rm tr}\left[F_L^{\mu\nu} U F_{R\mu\nu} U^\dagger\right] \ , \end{aligned} \tag{35}$$

where the last two (non-minimal) terms are necessary to achieve a satisfactory phenomenology in the vacuum. After the identifications $\rho^\mu \equiv V^\mu{=}A^\mu_R + A^\mu_L$, $A^\mu{=}A^\mu_R - A^\mu_L$ (and a field redefinition of the axialvector field to remove a $\partial^\mu\vec{\pi}A^\mu$ term), the leading terms of the MYM Lagrangian take the form

$$\begin{aligned} \mathcal{L}_{\rm mym} \ &= \ \frac{1}{2}m_\rho^2\vec{\rho}_\mu^{\,2} + \frac{1}{2}\left[m_\rho^2 + g^2 f_\pi^2\right]\vec{a}_{1\mu}^{\,2} + g^2 f_\pi \vec{\pi}\times\vec{\rho}^{\,\mu}\cdot\vec{a}_{1\mu} + \\ &\quad g^2_{\rho\pi\pi}\left[\vec{\rho}_\mu^{\,2}\vec{\pi}^2 - \vec{\rho}^{\,\mu}\cdot\vec{\pi}\ \vec{\rho}_\mu\cdot\vec{\pi}\right] + g_{\rho\pi\pi}\vec{\rho}_\mu\cdot(\vec{\pi}\times\partial^\mu\vec{\pi}) + \ldots \end{aligned} \tag{36}$$

($g^2_{\rho\pi\pi}{=}\frac{1}{2}g^2$). Note that the Higgs mechanism induces the *splitting* of ρ and a_1 masses,

$$m_{a_1}^2 = m_\rho^2 + g^2 f_\pi^2 \ , \quad m_\rho^2 = m_0^2 \ , \tag{37}$$

which is entirely due to SBχS (via f_π). The bare ρ mass itself is an *external* parameter, which is different from the HLS scheme discussed in the previous section. Electromagnetism is readily included into the MYM Lagrangian by adding the vector dominance coupling [91]

$$\mathcal{L}_{\rho\gamma} = \frac{em_\rho^2}{g_{\rho\pi\pi}} \ B_\mu \ \rho_3^\mu \ , \tag{38}$$

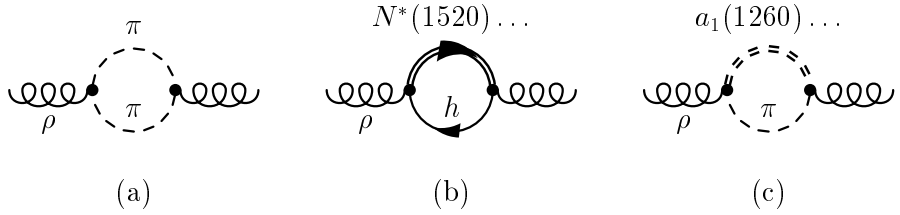

Figure 10: *Graphical representation of self-energy diagrams characterizing the interactions of the ρ meson in hot and dense hadronic matter: (a) renormalization of its pion cloud due to modified pion propagators, and direct interactions of the ρ meson with (b) baryons and (c) mesons, typically approximated by baryon- and meson-resonance excitations [94, 30].*

where B_μ denotes the photon field. In this scheme, VDM remains valid in the medium, and the task of computing the low-mass isovector axial/-vector correlators amounts to assessing the medium modifications of ρ and a_1 mesons.

The ρ-meson propagator in hot and dense hadronic matter can be written as

$$D_\rho^{L,T}(q_0,q;\mu_B,T)=\frac{1}{M^2-m_V^2-\Sigma_{\rho\pi\pi}^{L,T}-\Sigma_{\rho M}^{L,T}-\Sigma_{\rho B}^{L,T}}\ , \tag{39}$$

with transverse and longitudinal modes as defined in Eq. (25). The key quantities are the in-medium selfenergies, $\Sigma_\rho^{L,T}$, which may be classified as follows (cf. Fig. 10): $\Sigma_{\rho\pi\pi}$ accounts for the pion cloud of the ρ, which in the vacuum gives rise to its finite width via $\rho\to\pi\pi$. Direct interactions of the ρ with mesons (M=π, K, ρ, ...) and baryons (B=N, Λ, Δ, ...) from the heat bath are represented by $\Sigma_{\rho M}$ and $\Sigma_{\rho B}$, respectively; they vanish in the vacuum. In terms of underlying scattering processes, the latter are typically resonance excitations (e.g., $\rho\pi\to a_1$ or $\rho N\to N(1520)$) while medium modifications of pions (e.g., $\pi N\to\Delta$) in $\Sigma_{\rho\pi\pi}$ correspond to, e.g., t-channel π exchange processes ($\rho N\to\pi\Delta$). When evaluating interactions which are not directly constrained by chiral (or gauge) symmetry (especially those involving higher resonances), phenomenological information is essential for a reliable determination of the coupling constants (and cutoff parameters in the hadronic formfactors to account for the finite size of the hadrons). The simplest form of such constraints are hadronic decay widths of resonances (e.g., $a_1\to\rho\pi$), supplemented by radiative decays (e.g., $a_1\to\gamma\pi$). However, especially for "subthreshold" states (e.g., $\omega\to\rho\pi$ or $N(1520)\to\rho N$), where the coupling is realized via the low-energy ($\pi\pi$ decay) tail of the ρ spectral function, empirical information can be rather uncertain. In this case, comprehensive constraints inferred from scattering data become invaluable. Unfortunately, in practice this is only possible for ρN interactions (e.g., via $\pi N\to\rho N$ or γN scattering), but, as it turns out, the modifications of the ρ due to interactions with nucleons are generally stronger than with pions. In addition, by using nuclear targets, one has the possibility to constrain (or test) the modifications in nuclear *matter*, rather than on a single nucleon (which corresponds to the leading-order density effect).

Let us start by discussing finite-T effects. Calculations of the ρ propagator in a hot pion gas based on the MYM scheme [95] have shown small medium effects. An extended analysis [96] of the ρ in hot meson matter, including resonance excitations ($\rho\pi\to a_1,\omega,h_1,\pi',a_2(1320)$, $\rho K\to K^*,K_1$, $\rho\rho\to f_1(1285)$) and pion Bose enhancement in $\Sigma_{\rho\pi\pi}$, leads to total broadening of $\sim$80 MeV at T=150 MeV (corresponding to a pion density ϱ_π=0.12 fm$^{-3}\simeq$0.75 ϱ_0), with little mass shift. Approximately $\sim$20 MeV of

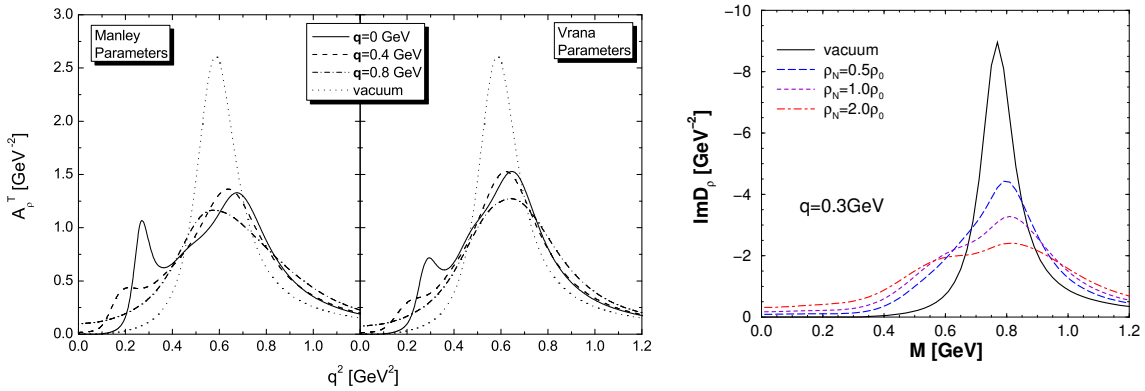

Figure 11: *Comparison of ρ-meson spectral functions in cold nuclear matter within the hadronic many-body approaches of Refs. [100] (left panels, based on two different phase shift analysis of πN scattering [101, 102]) and [94, 30] (right panel).*

the broadening is due to the $\pi\pi$ Bose factor (cf. also Ref. [97]) and ∼50-60 MeV due to meson resonances. The latter is comparable to Refs. [98, 99] which are directly based on $\rho\pi$ and ρK scattering amplitudes.

Next, we turn to modifications in cold nuclear matter. Fig. 11 shows two calculations in which the underlying ρ self-energies have been rather thoroughly constrained. In Ref. [100] (left panels), a ρN resonance model (corresponding to $\Sigma_{\rho N}$) has been constructed utilizing a detailed analysis of empirical $\pi N \to \rho N$ phase shifts and inelasticities [101, 102]. The resulting ρ spectral functions are displayed at normal nuclear density (taken as ϱ_N=0.15 fm^{-3}) for various three-momenta and two distinct data sets for constraints. A substantial broadening of close to ∼200 MeV is found, with a slight upward peak shift of a few tens of MeV; the three-momentum dependence is relatively weak. In Refs. [94, 30], $\Sigma_{\rho N}$ and an in-medium pion cloud, $\Sigma_{\rho\pi\pi}$ (incorporating P-wave "pisobar" nucleon- and Δ-hole excitations and associated vertex corrections), have been calculated

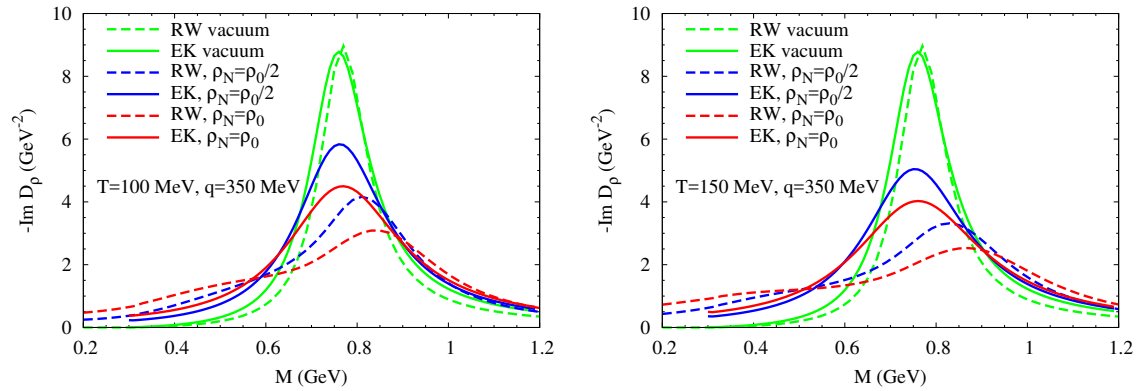

Figure 12: *Comparison of ρ-meson spectral functions in hot and dense hadronic matter from Refs. [30] (dashed lines) and [99] (solid lines) at temperatures of T=100 MeV (left panel) and T=150 MeV (right panel) for* nucleon *densities of ϱ_N=0.5,1.0 ϱ_0 (the corresponding nucleon chemical potentials are μ_N=673,745 MeV for T=100 MeV and μ_N=436,542 MeV for T=150 MeV, respectively).*

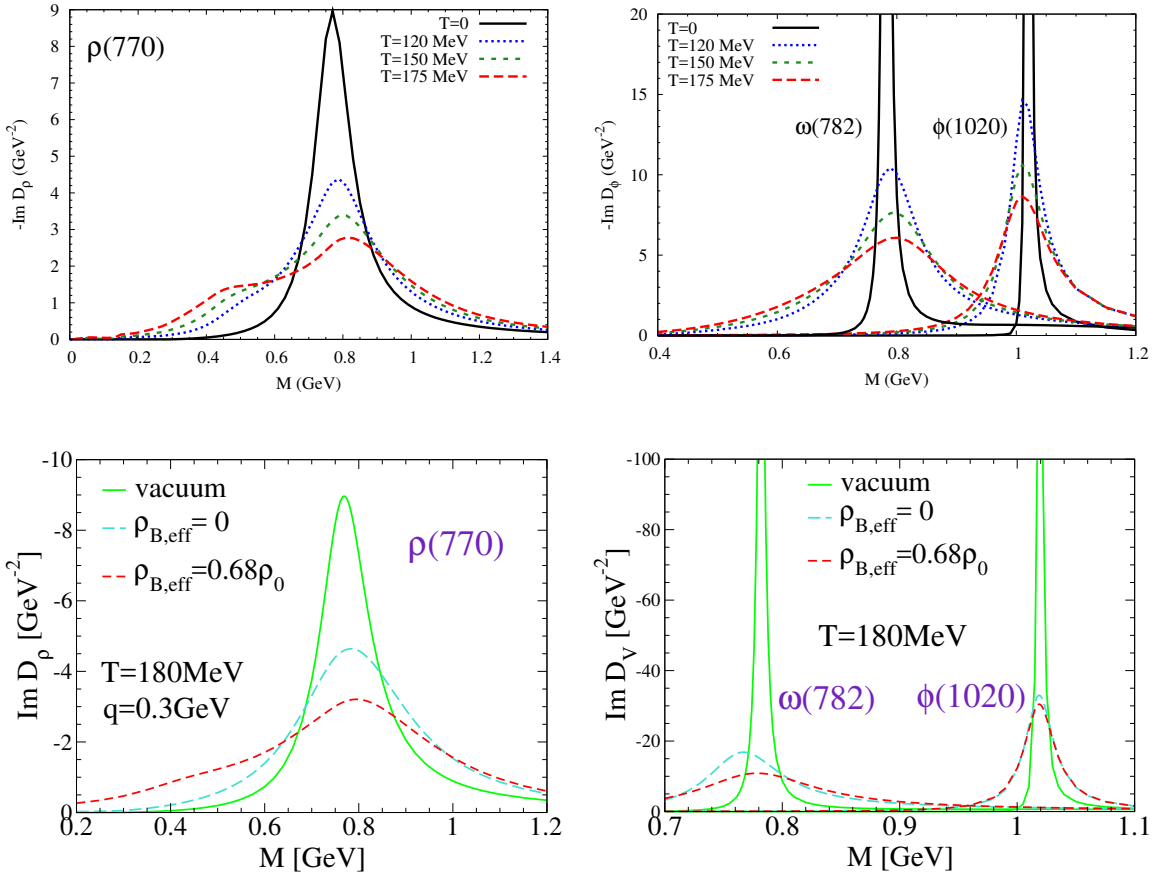

Figure 13: *In-medium spectral functions of light vector mesons in hot and dense hadronic matter based on the hadronic many-body approach of Refs. [103, 30, 105]; upper panel: under conditions resembling heavy-ion collisions at SPS (i.e., along an isentropic trajectory in the phase diagram which preserves the measured hadron ratios determined at* $(\mu_B^{\rm chem}, T_{\rm chem}) \simeq (230, 175)$ *MeV) [106]; lower panels: at* $(\mu_B, T) \simeq (25, 180)$ *MeV (resembling chemical freeze-out at RHIC) with (short-dashed lines) and without (long-dashed lines) medium effects induced by anti-/baryons [20].*

and constrained by total photoabsorption data on the nucleon and nuclei [103], as well as total $\pi N \to \rho N$ cross sections. The resulting spectral functions are quite similar to the ones of Ref. [100], with a somewhat stronger broadening of $\sim$300 MeV at ϱ_N=0.16 fm^{-3} and a comparable mass shift of $\sim$40 MeV. It is quite remarkable that the predicted in-medium mass and width of $\sim$(810,450) MeV are in good agreement with the QCD sum rule constraints derived in Ref. [87], cf. right panel in Fig. 8. Both broadening and mass shift decrease at higher three-momentum, e.g., $(\Delta m_\rho, \Delta\Gamma_\rho) \simeq$(30,150) MeV at q=1 GeV. Both calculations [100, 94] include a rather strong coupling to $\rho N(1520) N^{-1}$ excitations (appearing as a low-mass peak or shoulder in the ρ spectral function). This has been questioned in Ref. [104] based on a coupled channel analysis of S-wave ρN and ωN scattering, where all nucleon resonances but the $\Delta(1232)$ are generated dynamically via four-point interactions. The (generated) $N(1520)$ is deduced to primarily couple to ωN rather than ρN, entailing an in-medium ρ with significantly less broadening.

Finally, we turn to a hot and dense hadronic medium as expected to be formed in high-

energy heavy-ion collisions. In Fig. 12 the ρ spectral functions of the hadronic many-body calculations [94, 30] are compared to those obtained in the scattering-amplitude approach of Ref. [99]. The latter exhibit less broadening and a small (if any) downward mass shift of the ρ peak, compared to the upward shift in the many-body approach (mostly induced by baryonic effects). Consequently, in terms of spectral strength, the discrepancies between the two calculations are largest for masses around $M\simeq 0.7\,\mathrm{GeV}$, as well as for very low mass, $M\leq 0.4\,\mathrm{GeV}$, by up to a factor of $\sim$2. This mass region is much magnified in thermal dilepton production rates due to the Boltzmann factor and a photon propagator $\propto 1/M^2$. However, the amplitude approach only accounts for interactions with pions and nucleons, while the many-body calculations include estimates of ρ interactions with strange baryons and resonances [30]. This difference may account for some of the discrepancy.

In preparation for applications to dilepton spectra in URHICs, we summarize in Fig. 13 in-medium V-meson spectral functions in the many-body approach under conditions relevant for SPS (upper panels) [30, 106] and RHIC (lower panels) [105]. The ρ meson (left panels) "melts" when extrapolated to temperatures close to the expected phase boundary. Baryons play an essential role in the melting, even at RHIC (where the net baryon density is small), since the relevant quantity is the *sum* of baryon and antibaryon densities. The effects due to baryons and antibaryons are most prominent as an enhancement in the mass region below $M\simeq 0.5\,\mathrm{GeV}$. The ω and especially ϕ spectral functions (right panels) appear to be more robust. One should also point out that at T=120,150 MeV in the upper panels appreciable pion and kaon chemical potentials are present which sustain larger hadron densities and thus support stronger medium effects than in chemical equilibrium.

3.5 Thermal Dilepton and Photon Rates

The in-medium vector-meson propagators discussed in the preceding section are converted to thermal dilepton rates via Eqs. (20) (upper line) and (13). This is based on the assumption that VDM for the EM correlator remains valid in the medium[8]. The resulting three-momentum integrated thermal dilepton rates are summarized in Fig. 14. The left panel, which displays the isovector channel, reiterates that the ρ resonance signal disappears from the mass spectrum as one approaches the putative phase boundary. The hadronic rates also include an estimate of the leading-T chiral mixing effect, Eq. (22), in the mass region M=1-1.5 GeV. The comparison to perturbative $q\bar{q}$ annihilation reveals that the the top-down extrapolated QGP rate closely coincide with the bottom-up extrapolated in-medium hadronic one, especially in case of the HTL-improved $q\bar{q}$ rate. This feature suggests that the hadronic rate has indeed approached χSR (since the QGP rates are chirally symmetric at any finite order in perturbation theory) [34, 30]. The "matching" of QGP and hadronic rates occurs directly in the timelike regime without the need for in-medium changes of the bare parameters in the effective Lagrangian. Medium effects due to baryons play an important role in this mechanism; the situation is similar for small μ_B and close to T_c where the sum of baryon and antibaryon densities is appreciable, see right panel of Fig. 14. ω and especially ϕ mesons appear to be more robust, possibly surviving above T_c. The dilepton rates in the vector manifestation of HLS [93] look rather different; based on the pertinent pion EM formfactor, Fig. 9, a distinct ρ peak survives in the rate up to temperatures of at least $T=0.85\,T_c\simeq 155\,\mathrm{MeV}$ (assuming $T_c\simeq 180\,\mathrm{MeV}$).

[8]Strictly speaking, the EM correlator of Refs. [94, 30] includes corrections to VDM in the baryon sector as determined via photoabsorption spectra on the nucleon and nuclei [103]; the assumption is that this modified version of VDM is not affected at higher densities and at finite temperature.

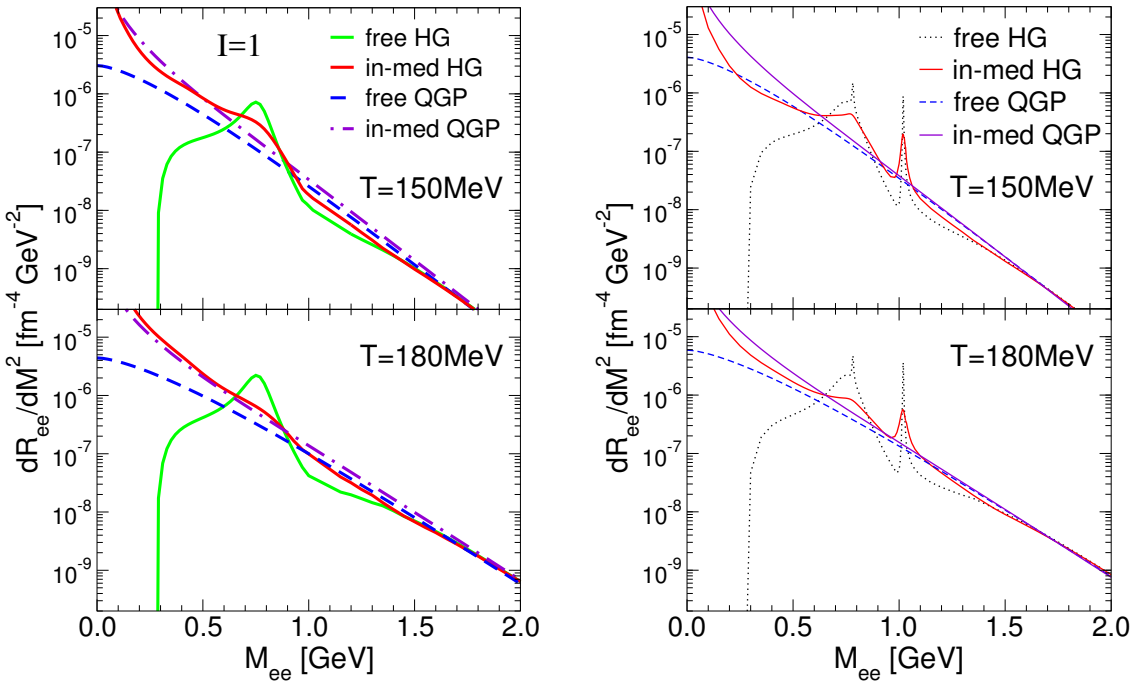

Figure 14: *Three-momentum integrated thermal dilepton rates at fixed temperature [70, 107] for the vacuum ρ (dotted lines), the hadronic many-body approach of Refs. [103, 30] (solid lines) and for the QGP using either free $q\bar{q}$ annihilation (dashed line) or hard-thermal loop improved rates [78] (dash-dotted line). The left panel refers to the isovector (ρ) channel, under conditions resembling heavy-ion collisions at the SPS (fixed μ_B=270 MeV). The right panel additionally includes isoscalar (ω and ϕ) channels and corresponds to small $\mu_B \simeq 25$ MeV appropriate for the conditions at collider energies.*

Emission rates of dileptons are closely related to those of real photons which are determined by the lightlike limit ($q_0 = \mid \vec{q} \mid$) of the EM spectral function,

$$q_0 \frac{dN_\gamma}{d^4x d^3q} = -\frac{\alpha_{\rm em}}{\pi^2} \; f^B(q_0;T) \; \mathrm{Im}\,\Pi_{\rm em}(M=0,q;\mu_B,T) \; . \tag{40}$$

In Ref. [108] the in-medium ρ of Refs. [103, 30] has been found to constitute the dominant hadronic source of thermal photons for momenta up to $q \simeq 1$ GeV; above, t-channel meson exchange reactions not included in the spectral function (most notably π and ω exchange in $\pi\rho \to \pi\gamma$) take over, cf. left panel of Fig. 15. Similar to the dilepton case, at temperatures of 150-200 MeV, the strength of the combined thermal rate for hadronic photon production turns out be very comparable to perturbative QGP emission, especially for the complete leading-order result [110].

4 Interpretation of Dilepton Spectra

In this section we will scrutinize experimental results for dilepton spectra in light of the theoretical developments elaborated above. A brief discussion of production experiments off nuclei, representing cold nuclear matter up to saturation density, will be followed by

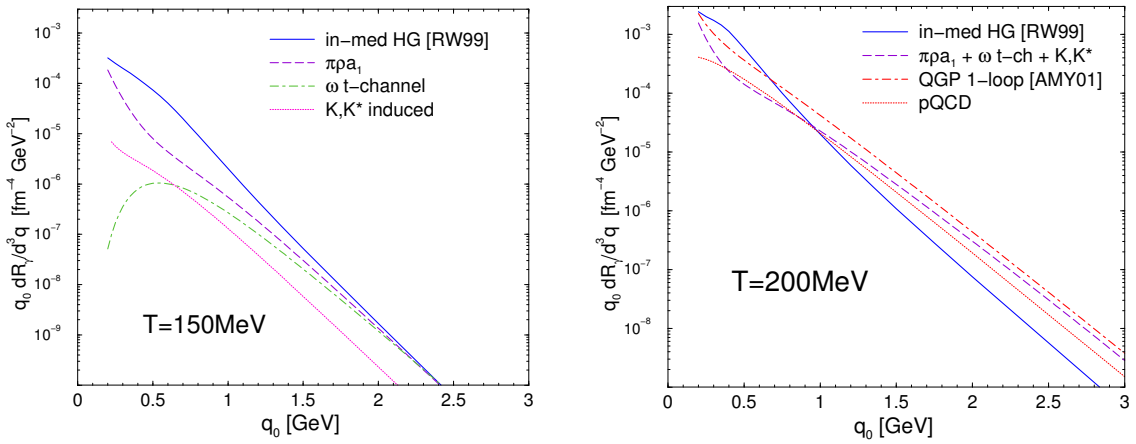

Figure 15: *Thermal photon production rates in hot hadronic matter [108] (left panel), and compared to 1-loop [109] and full leading-order [110] QGP emission (right panel).*

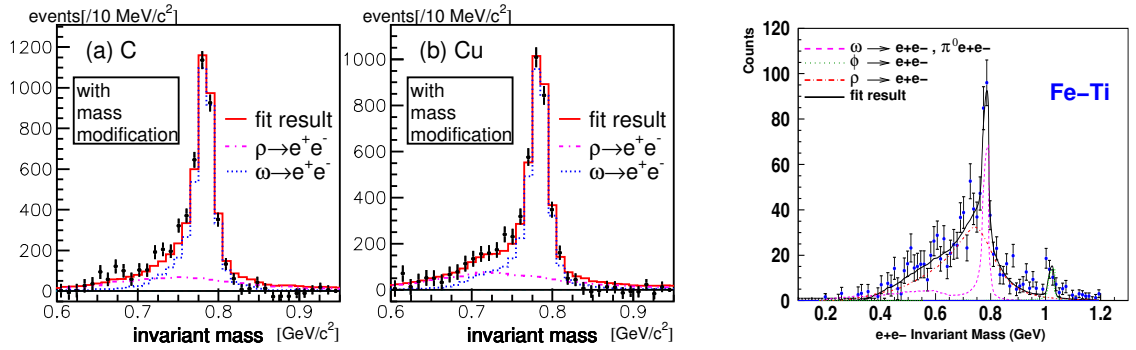

Figure 16: *Invariant-mass spectra of e^+e^- in proton- (left) [46] and photon-induced (right) [45] reactions off nuclear targets.*

a more extensive study of invariant-mass and momentum spectra in heavy-ion reactions involving hot and dense matter possibly probing the transition regime to the QGP.

4.1 Medium Effects in Nuclei

Dilepton production experiments off nuclei have the advantage over heavy-ion collisions that the medium is well-defined. Medium- to heavy ground-state nuclei resemble in their interior infinitely extended nuclear matter at vanishing temperature. Therefore the experiments probe to a large extent the properties of "cold nuclear matter". However, a good knowledge of the production process is required, and medium effects are typically rather moderate, further reduced by surface effects and decays outside the nucleus especially at large three-momenta (which, in turn, are needed in the production process).

The E325 experiment at KEK [46] used 12 GeV proton projectiles and found significant differences in the spectra between C and Cu targets, see left panel of Fig. 16. After subtraction of combinatorial background as well as η and ω Dalitz decays, the best fit to the excess spectra using ω and ρ Breit-Wigner distributions was obtained with a mass shift of ca. 9% at nuclear matter density, and a ρ/ω ratio of about $\sim$0.45.

The CLAS experiment [45] used a photon beam at Jefferson Lab with incident energies E_γ=0.6-3.8 GeV, directed on various nuclear targets. After subtraction of the

combinatorial background, determined with absolute normalization, the invariant-mass spectra are best reproduced with a ρ spectral distribution with a mass and width of (m_ρ,Γ_ρ)=(775±5,220±15) MeV, cf. right panel of Fig. 16. These values are well reproduced by Boltzmann transport calculations [111], and are consistent with the predictions of Refs. [94, 30] at ϱ_N=0.5 ϱ_0 and q=1 GeV, where $(\Delta m_\rho, \Delta\Gamma_\rho)\simeq$(15,75) MeV, see Ref. [112] for a recent calculation. An apparent difference between the E325 and CLAS spectra is that the background subtraction in the former removes any excess for $M\simeq$0.85-1 GeV; this suppresses (and possibly shifts down) the ρ contribution in the E325 fit.

Photoproduction experiments (E_γ=0.8-1.12 GeV) of P-wave $\pi^+\pi^-$ pairs off ^{2}H, ^{3}He and ^{12}C were conducted by the TAGX collaboration [113]. The spectra for the ^{12}C target support medium effects in line with hadronic many-body ρ spectral functions [94, 30].

4.2 Heavy-Ion Collisions

In contrast to production experiments off nuclei, the (energy-) density of the medium created in heavy-ion collisions undergoes a rapid evolution after initial nuclear impact until break-up. Even under the simplifying assumption of local thermal equilibrium, a good knowledge of the temperature and baryon-density evolution is necessary to convert the dilepton rates discussed above into a space-time integrated spectrum In addition, sources other than thermal radiation have to be considered, especially toward higher mass *or* q_t where the assumption of equilibrium becomes increasingly questionable. These issues are addressed in Sec. 4.2.1. Phenomenological analyses of dilepton spectra focus on recent SPS data from NA60 and CERES/NA45 in Secs. 4.2.2 and 4.2.3, respectively, with a short digression to direct photons (W98) and a brief outlook to future experiments in Sec. 4.2.4.

4.2.1 Thermal Evolution and Dilepton Sources

As discussed in Sec. 1.2, hadronic observables in URHICs point at a reasonable degree of thermalization of the bulk medium produced in these reactions. Therefore, we here focus on hydrodynamic and expanding fireball approaches utilizing the assumption of local thermal equilibrium.[9]

Thermal emission spectra follow from the convolution of the production rate, Eq. (13), over the space-time evolution of the medium,

$$\frac{\mathrm{d}N_{ll}}{\mathrm{d}M\mathrm{d}y} = \frac{M}{\Delta y}\int_0^{\tau_{\rm fo}} \mathrm{d}\tau \int_{V_{\rm FB}} \mathrm{d}^3x \int \frac{\mathrm{d}^3q}{q_0}\, \frac{\mathrm{d}N_{ll}}{\mathrm{d}^4x\,\mathrm{d}^4q}(M,q;T,\mu_N,\mu_s,\mu_i)\ \mathrm{Acc}(M,q_t,y), \qquad (41)$$

where $\mathrm{Acc}(M,q_t,y)$ accounts for the detector acceptance and Δy denotes the corresponding rapidity interval. The temperature and chemical potentials in general depend on space-time, $(\tau,\vec{x})$. Note that while μ_N and μ_s correspond to exact conservation of baryon number and strangeness, effective chemical potentials $\mu_i = \mu_{\pi,K,\eta,...}$ are needed to preserve the experimentally observed hadron ratios in the evolution of the hadronic phase between chemical ($T_{\rm ch}$=155-175 MeV) and kinetic freezeout ($T_{\rm fo}$=100-140 MeV).

An overview of several key input parameters of three thermal approaches [36, 106, 117, 118, 119, 120], which have been used to compute dimuon spectra in comparison

[9] Comparisons of dilepton spectra computed in hydrodynamic/fireball and transport calculations (based on similar in-medium spectral functions) have shown rather good agreement, see e.g. Refs. [114, 30], Ref. [115], or Refs. [106, 116].

	DZ	RR	HR
T_0	220 MeV (peak)	250 MeV (peak)	190 MeV (average)
T_c	170 MeV	170 MeV	175(160/190) MeV
$T_{\rm fo}$	130 MeV	130 MeV	120(135) MeV
spatial	Glauber (initial)	Woods-Saxon	isotropic
$v_{\rm fo}^{\rm s}$	∼0.5-0.55	0.57	0.53
$v(r)$	approx. linear	$\rho_t \propto \sqrt{r}$	$v_t \propto r$
$\tau_{\rm FB}$	$\sim$ 8-9 fm/c	$\sim$ 7.5 fm/c	$\sim$ 6.5 fm/c
QGP-EoS	massless (N_f=3)	quasi-particle model	massless (N_f=2.3)
HG-EoS	lowest SU(3) multipl.	$m_{B,M} \leq$ 2, 1.5 GeV	$m_{B,M} \leq$ 2, 1.7 GeV
s/ϱ_B	42	26(?)	27
$\mu_\pi^{\rm fo}$	0	? ($\neq$ 0)	80(35) MeV
EM rates	chiral virial	empirical scatt. ampl.	hadronic many-body

Table 1: *Fireball parameters employed in the calculations of dilepton spectra in In(158 AGeV)-In collisions in Refs. [117, 118] (DZ), [119, 120] (RR) and [36, 106] (HR).*

to NA60 data, is compiled in Tab. 1 (see also Ref. [125]). The overall range of the underlying parameters and assumptions is rather similar. This is not a coincidence but a consequence of constraints from measured hadron spectra at SPS energies [121, 122, 123, 124] which all of the three models have been subjected to. There are, however, noticeable differences. E.g., all approaches operate with a for SPS energies "canonical" formation time of τ_0=1 fm/c, but the initial peak temperature in Ref. [120] is about 15% larger than in Ref. [117] (e.g., due to differences in the underlying QGP EoS). Averaging over the initial spatial density profile typically leads to a 15% smaller *average* temperature [126]; thus, $\bar{T}_0 \simeq$190 MeV in Ref. [36] is quite consistent with $T_0^{\rm max} \simeq$220 MeV in Ref. [117]. The slightly larger expansion velocity in Ref. [120] (surface velocity $v_{\rm fo}^{\rm s}$=0.57 at thermal freezeout), together with its square-root radial profile, imply larger boost factors in the q_t spectra which becomes significant at high momenta. In this approach preliminary NA60 pion spectra in semicentral In-In are saturated by thermal emission over the entire measured range up to $p_T \simeq$3 GeV. Alternatively, in Ref. [106], based on an analysis of pion spectra in Pb-Au and S-Au collisions at SPS, the thermal component was found to account for the pion yields only up to $p_T \simeq$1 GeV, requiring the introduction of a "primordial" component associated with initial hard scattering of the incoming nucleons. This interpretation is supported by the observation that the pion spectra for $p_T \geq$2 GeV essentially scale with the number of binary N-N collisions ($N_{\rm coll}$), indicating that the hard component dominates the spectra at these momenta. The preliminary NA60 pion spectra are also well predicted in this approach, with a crossing of thermal and hard components at $p_T \simeq$1.2 GeV. As discussed in Sec. 1.2, a valuable indicator of the degree of thermalization is the elliptic flow, $v_2(p_T)$. At SPS energies, ideal hydrodynamics overpredicts this quantity even at low p_T by about 30-50% (possibly due to neglecting effects of finite viscosity, in connection with initial temperatures in the vicinity of T_c where the EoS is presumably rather soft). Moreover, the experimental $v_2(p_T)$ in semicentral Pb-Au levels off at p_T=1.5-2 GeV [127, 128], indicative for a transition to a kinetic regime, while hydrodynamic results keep rising, overpredicting $v_2(p_T$=2 GeV) by about a factor of ∼2.

Concerning effective chemical potentials for pions (and other stable particles) between

chemical and thermal freezeout, their main effect is a faster cooling in the evolution of $T(\tau)$ (the equation of state, $P(\epsilon)$, is largely unaffected) [129, 130]. E.g., for μ_π=80 MeV at T=120 MeV [36], the pion density, $\varrho_\pi(T,\mu_\pi)$, is enhanced by a factor of $\sim e^{80/120}\sim 2$ relative to μ_π=0, and as large as ϱ_π(T=150 MeV,0). Therefore, thermal freezeout at $(T_{\rm fo},\mu_\pi^{\rm fo})$=(130,0) MeV [117] corresponds to a smaller pion density (and thus larger volume) than at $(T_{\rm fo},\mu_\pi^{\rm fo})$=(120,80) MeV [36], consistent with the longer lifetime in Ref. [117].

Implications of varying critical and chemical-freezeout temperatures for dilepton spectra have been studied in Ref. [106]. The value of T_c affects the *relative* partition of QGP and hadronic emission, especially at masses $M\geq$1 GeV where the Boltzmann factor augments the sensitivity to earlier phases and the hadronic rates are not enhanced by resonances. However, if hadronic and QGP rates are "dual" around T_c, this distinction is largely academic. Smaller $T_{\rm ch}$'s lead to smaller μ_i's in the subsequent hadronic evolution, and thus higher kinetic freezeout temperatures, e.g., $(T_{\rm fo},\mu_\pi^{\rm fo})$=(135,35) MeV for $T_{\rm ch}$=160 MeV.

Experimentally measured dilepton spectra contain sources other than thermal radiation represented by Eq. (41). A systematic evaluation of these sources has recently been conducted in Ref. [106], in terms of (i) final-state decays and (ii) primordial sources.

Dilepton decays of long-lived hadrons (mostly η, η', ω and ϕ mesons) after thermal freezeout, commonly referred to as "hadron decay cocktail", are usually based on chemical freezeout for their abundance and thermal freezeout for their p_T spectra. The situation is more involved for the ρ-meson, since its continuous regeneration implies relative chemical equilibrium with pions until thermal freezeout (to a certain extent this may also apply to ω and ϕ) . In addition, its short lifetime is not well separated from the typical duration of the freezeout process. In Ref. [30], the final generation of ρ decays has been approximated by an extra 1 fm/c of fireball lifetime. However, as has been clarified in Refs. [131, 106], when treating the final generation of ρ's as a cocktail decay, the time dilation of the moving ρ's generates a hardening of its q_t spectrum by a factor γ_t=M_t/M (M_t^2=M^2+q_t^2). The resulting spectrum recovers the standard Cooper-Frye [132] description for freezeout at a fixed time in the laboratory frame (cf. also Refs. [133, 134]). This, in turn, implies that the apparent temperature of the radiation formula (41) is smaller than the actual temperature figuring into the Boltzmann factor (independent of flow effects) by about $\sim$10%.[10]

In analogy to the pion-p_T spectra discussed above, the ρ spectra are expected to have a primordial component (emanating from hard N-N collisions) which does not equilibrate with the medium. Such a component has been introduced in Refs. [131, 106] including a schematic treatment for Cronin effect and jet-quenching as inferred from pion spectra in S-Au and Pb-Au collisions at SPS [135] (also note that, at high q_t, this component scales with $N_{\rm coll}$, rather than $N_{\rm part}$ as for the (low-p_T) cocktail).

Another primordial dilepton source is the well-known Drell-Yan (DY) process, i.e., quark-antiquark annihilation in binary N-N collisions. To leading order $q\bar{q}\to e^+e^-$ is $\mathcal{O}(\alpha_s^0\alpha^2)$ and can be reliably calculated in perturbation theory at sufficiently large masses, $M\gtrsim$2 GeV, utilizing parton distribution functions as input [136]. A finite pair momentum, q_t>0, can be generated by intrinsic parton k_t and at next-to-leading order (NLO) (the latter is the dominant effect). The extrapolation of DY to small masses is problematic, but at a scale of $q_t\simeq$2 GeV its contribution to dilepton spectra at SPS is potentially sizable. In Ref. [106] it has been suggested to estimate the spectrum of slightly virtual DY pairs, i.e., for $M^2\ll q_t^2$, by an extrapolation of a finite-q_t DY expression to zero mass and constrain the resulting photon spectrum by measured photon spectra in p-A collisions.

[10] The time dilation factor for ρ decays in the thermal radiation formula is compensated by the same time dilation in ρ formation, as a consequence of detailed balance.

Semileptonic final-state decays of correlated of D and $\bar{D}$ mesons (i.e., corresponding to an associately produced $c\bar{c}$ pair) lead to an irreducible dilepton signal. The pertinent mass spectrum is, in fact, sensitive to reinteractions of the charm quarks and/or hadrons in the medium. At SPS energies, the relevance of this effect for correlated $D\bar{D}$ decays is currently an open question [137]. Theoretical calculations discussed in the following are employing N_{coll}-extrapolated spectra from p-p collisions (based on PYTHIA [139] simulations) as provided by the NA60 collaboration [35].

4.2.2 CERN-SPS I: NA60

In section we discuss several calculations of $\mu^+\mu^-$ spectra in semicentral In(158 AGeV)-In collisions as measured by NA60. The excellent mass resolution and statistics of the data allowed for a subtraction of the hadronic cocktail (excluding ρ and $D\bar{D}$ decays), resulting in the so-called "excess spectra" (in more recent, acceptance-corrected, NA60 spectra [138] correlated $D\bar{D}$ decays are also subtracted, with some caveat as to their medium modifications, as mentioned above).

Theoretical predictions [20] of the low-mass excess spectra utilizing the in-medium ρ spectral function of Ref. [30] (cf. Sec. 3.4.2) showed good agreement with the first data of NA60 [35]. More complete calculations including QGP radiation (as in Ref. [140] but with hard-thermal loop resummed rates [78]), in-medium ω and ϕ decays [105], 4π-like annihilation (relevant at intermediate mass) [36], as well as primordial ρ and Drell-Yan (DY) contributions (relevant at high q_t), are summarized in Fig. 17. In connection with a slight update of the fireball model (larger acceleration implying smaller lifetime), the resulting description of the NA60 invariant-mass spectra is quite satisfactory over the entire range, including projections onto low (q_t<0.5 GeV) and high (q_t>1.0 GeV). In-medium ω and ϕ contributions are rather localized in mass, while QGP and DY radiation are at the 10-15% level at masses below 1 GeV. The in-medium plus freezeout (FO) ρ contributions [20] remain the dominant source confirming the notion that the NA60 low-mass data probe the in-medium ρ spectral function. This is also borne out of the acceptance-corrected q_t-spectra where, for M<1 GeV the ρ contribution prevails up to momenta of $q_t \simeq$ 1 GeV.[11] At q_t>1 GeV DY and primordial ρ-mesons become an increasingly important source, but the data for M=0.4-0.6 GeV and 0.6-0.9 GeV cannot be fully accounted for. These discrepancies are less pronounced for central In-In collisions, and may possibly be resolved by a stronger transverse expansion within the constraints of the hadronic spectra (we return to this question below). At masses M=1-1.4 GeV, the most significant sources are hadronic emission from multi-pion states (e.g., π-a_1, ρ-ρ or π-ω annihilation), QGP and $D\bar{D}$ decays. The hadronic contribution is significantly enhanced (by maximally a factor of $\sim$2 around $M\simeq$1 GeV) due to the effects of chiral mixing [36] (recall Sec. 3.2.1), which currently cannot be discriminated by the data. The q_t spectra for M=1-1.4 GeV are well described over the entire momentum range.

Fig. 18 summarizes the results of hydrodynamic calculations [117, 118] based on hadronic emission rates within the chiral-reduction approach [74, 75, 76] (cf. Sec. 3.2.1), freezeout ρ mesons (including the proper γ factor relative to thermal radiation) and perturbative $q\bar{q}$ annihilation in the QGP (pQGP). The overall structure of the NA60 mass spectrum is roughly reproduced (cf. upper left panel of Fig. 18), but the ρ resonance figur-

[11] The experimental q_t-spectra in Figs. 17, 18, 19 are not absolutely normalized; the theoretical q_t-spectra in Fig. 17 are normalized using the M-spectra at low q_t; however, whereas the experimental M-spectra for q_t>1 GeV are reasonably reproduced, the q_t-spectra for M=0.4-0.6 GeV are underestimated for q_t>1 GeV.

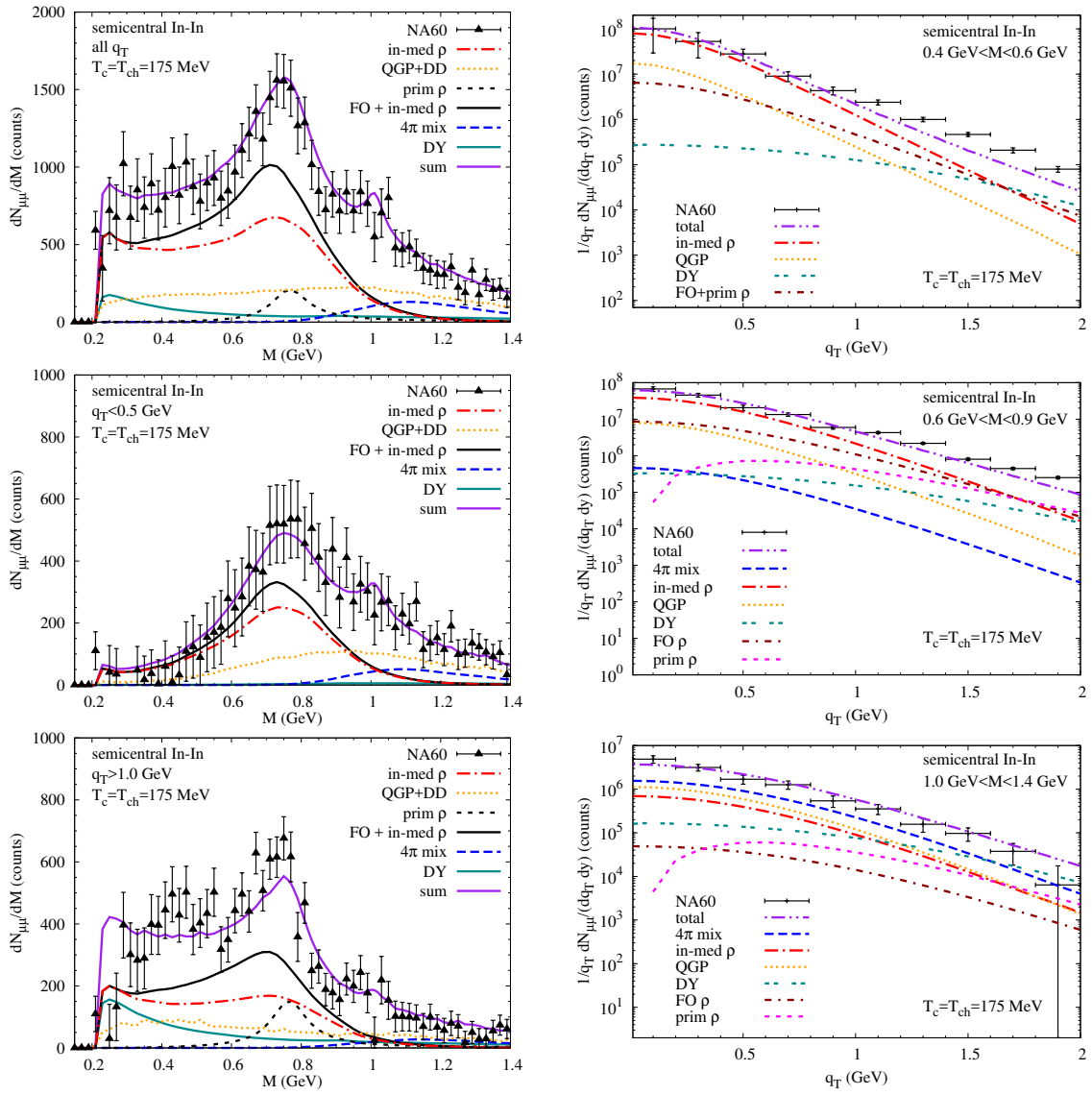

Figure 17: *Dimuon invariant-mass (left panels) and acceptance-corrected transverse-momentum (right panels) spectra in semi-central* In(158 AGeV)-In *collisions. Calculations [106] for thermal emission utilizing in-medium ρ, ω and ϕ spectral functions based on hadronic-many body theory [30, 105], 4π annihilation including chiral mixing [36] and QGP emission, supplemented by non-thermal sources (Drell-Yan annihilation, primordial and freeze-out ρ-meson, open-charm decays), are compared to NA60 data [35, 141, 142].*

ing into the EM correlator lacks significant in-medium broadening, despite the reduction in peak strength due to the mixing effect (the agreement improves for semiperipheral and peripheral collisions [117]). The freezeout-ρ contribution compares quite well with the one in the upper left panel of Fig. 17 which includes a broadening but also occurs at higher pion density (recall the discussion in Sec. 4.2.1). The level of the pQGP contribution is very similar to the fireball model of Refs. [36, 106] in Fig. 17. As in Refs. [36, 106] the hadronic contribution at M>1 GeV is based on a fit to the EM correlator in vacuum, but the mixing effect is less pronounced in the virial scheme, leading to a slightly smaller

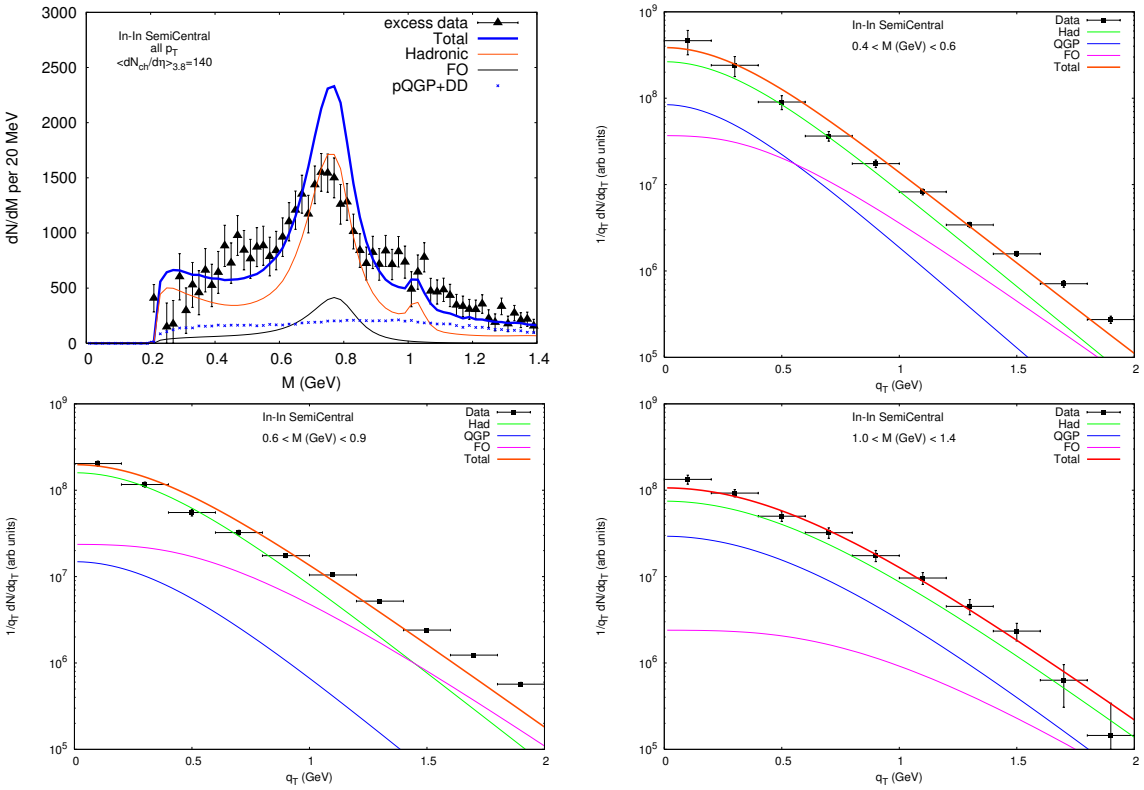

Figure 18: *NA60 dimuon spectra [35, 141, 142] compared to calculations [117, 118] employing thermal rates from the chiral reduction approach [75] and perturbative $q\bar{q}$ annihilation, folded over a hydrodynamic expansion for semicentral* In(158 AGeV)-In *collisions, supplemented with free ρ-meson decays after thermal freezeout. Upper left: M-spectra; other panels: q_t spectra in three mass bins.*

contribution in the dilepton spectrum (possibly also due to the absence of pion chemical potentials). The shapes of the q_t spectra (local slopes) of all 3 contributions displayed in Fig. 18 (in-medium hadronic, freezeout ρ and QGP) agree well with the fireball calculations of Refs. [36, 106] as demonstrated in a direct comparison in Ref. [141]. This suggests good consistency of the fireball and hydrodynamic evolution.

In Ref. [120] a thermal fireball expansion (cf. Tab. 1, middle column) has been applied to compute dimuon spectra utilizing in-medium ρ and ω spectral functions (based on empirical scattering amplitudes on pions and nucleons, recall solid lines in Fig. 12) [99], vacuum 4π annihilation (with both charged [144] and neutral pions), as well as QGP rates based on the quasiparticle model of Ref. [143], cf. Fig. 19. The overall shape and magnitude of the mass spectra is rather well reproduced, except close to the dimuon threshold where the importance of baryon effects is apparently underestimated (the underlying ρ spectral function at T=150 MeV shows little variation between baryon densities of ϱ_B=0.5 ϱ_0 and ϱ_0 [120]). The q_t spectra can be reasonably well described without contributions from DY or primordial ρ's, which differs from the hydrodynamic (DZ) [117, 118] and HR-fireball [36, 106] results, cf. Ref. [141] (recall that the RR fireball model describes NA60 pion spectra over the entire p_T range by thermal emission); part of this discrepancy is due to the slightly larger expansion velocity and the square-root radial profile of the transverse rapidity, cf. Tab. 1. Another significant difference concerns the magnitude of the QGP

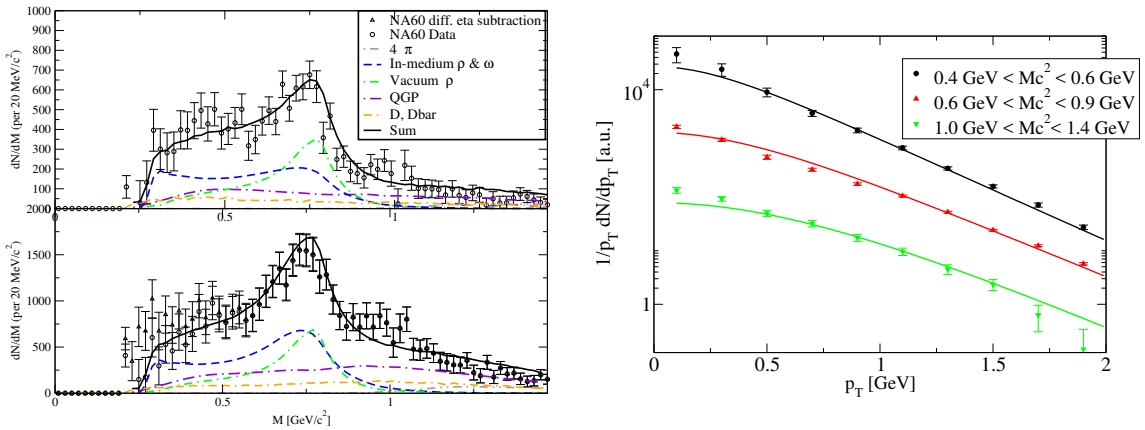

Figure 19: *NA60 dimuon spectra [35, 141, 142] compared to calculations [120] employing thermal rates with in-medium ρ and ω spectral functions [99] and free 4π annihilation in hadronic matter, as well as $q\bar{q}$ annihilation in the QGP [143], folded over a thermal fireball expansion for semicentral* In(158 AGeV)-In *collisions, supplemented with free ρ-meson decays after thermal freezeout. Left panel: M-spectra for all q_t (bottom) and for q_t>1 GeV (top); right panel: q_t spectra in three mass bins.*

contribution, which is by a factor of $\geq$2 larger in Ref. [120] than in Refs. [36, 117]. Part of this discrepancy is due to the quasiparticle QGP EoS employed in Ref. [120], which entails larger temperatures (including T_0) at given fireball volume. It is also related to the prevailing role of QGP radiation for $M \geq 1$ GeV.

The sensitivity of the NA60 data to the critical and chemical freezeout temperatures has been elaborated in Ref. [106], by varying T_c from 160-190 MeV and $T_{\rm ch}$ from 160-175 MeV (keeping the fireball expansion parameters fixed), representing current uncertainties in lattice QCD [4, 5] and thermal model fits [8, 9]. With "quark-hadron" duality

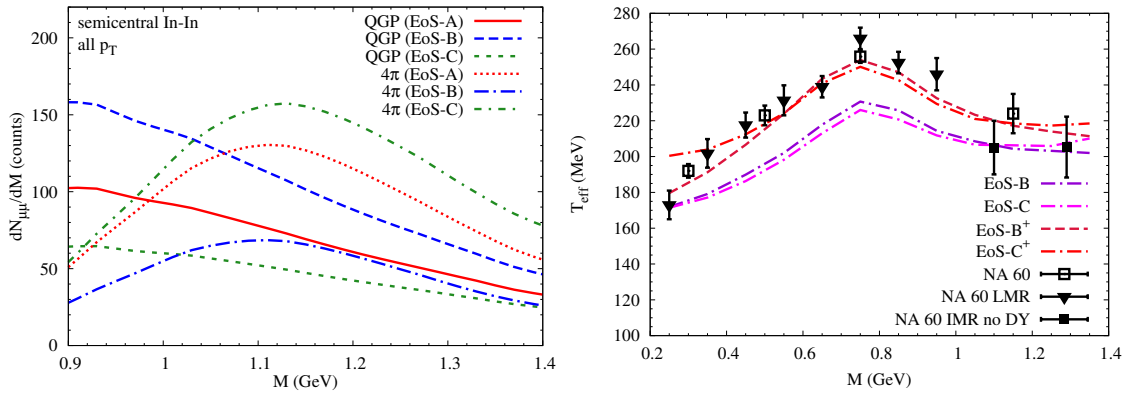

Figure 20: *Sensitivity of dilepton spectra to critical and chemical-freezeout temperature [106]. Left panel: QGP and hadronic (4π) radiation at intermediate mass for T_c=$T_{\rm ch}$=175 MeV (EoS-A), T_c=$T_{\rm ch}$=160 MeV (EoS-B) and (T_c,$T_{\rm ch}$)=(190,160) MeV (EoS-C); right panel: slope parameters in q_t-spectra for EoS-B and EoS-C (lower curves) and for 15% increased fireball expansion (EoS-B$^+$ and EoS-C$^+$, where the latter additionally includes ω t-channel exchange in $\pi\rho \to \pi e^+e^-$ reactions; all without Drell-Yan contribution); data are from Refs. [141, 142].*

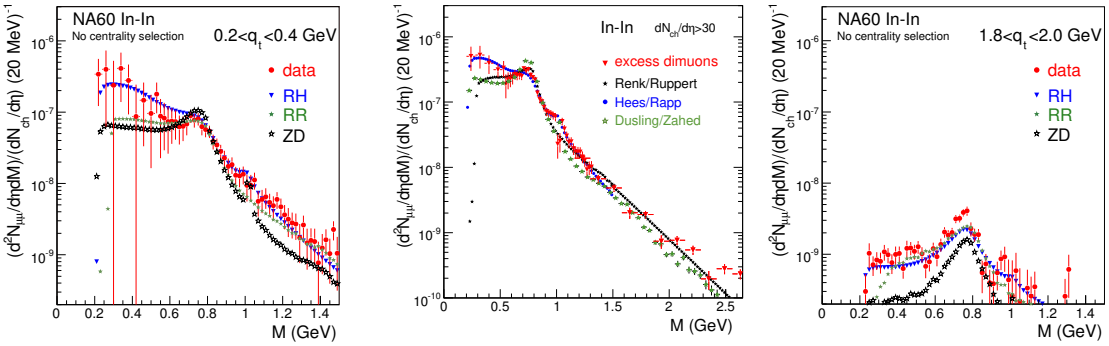

Figure 21: *Comparison of acceptance-corrected excess dimuon mass spectra (for 0.2<q_t/GeV<0.4 (left), q_t>0.2 GeV (middle) and 1.8<q_t/GeV<2.0 (right)) in minimum-bias* In(158 AGeV)-In *collisions [145, 137, 138] to model predictions for semicentral In-In of RH (EoS-A) [106], RR [120] and ZD [118], normalized to the average* $N_{\rm ch}$ *of the data.*

in the thermal dilepton rates [30] in this temperature regime (at *all* masses, cf. Fig. 14), the invariant-mass spectra turn out to be remarkably *in*sensitive to these variations [106] (duality of the QGP and hadronic emission for $M \lesssim 1.5$ GeV close to T_c is not realized in the rates underlying the calculations of Refs. [117, 120]). However, the partition of QGP and hadronic (4π) emission at intermediate masses changes appreciably from hadron-gas dominated spectra for $T_c \geq 175$ MeV to QGP dominated ones for T_c=160 MeV, cf. left panel of Fig. 20. In the latter case, the smaller value for $T_{\rm ch}$=160 MeV implies smaller chemical potentials in the hadronic phase. This is part of the reason for the reduction in hadronic emission, but also leads to a larger freezeout temperature by about 15 MeV (recall the discussion in Sec. 4.2.1 and right column in Tab. 1). This, in turn, helps in the description of the transverse-momentum spectra at q_t>1 GeV. However, an additional increase in the transverse fireball acceleration by 15% seems to be required to achieve quantitative agreement with the effective slope parameters as displayed in the right panel of Fig. 20. It remains to be checked whether this can be consistent with a more complete set of hadronic spectra in In(158 AGeV)-In collisions.

A comparison the three model calculations discussed above to acceptance-corrected mass spectra in minimum-bias In(158 AGeV)-In [145] in Fig. 21 reiterates the importance of baryon-driven medium effects [106] at low M and low q_t, as well as the lack of high-q_t yield in the ρ-mass region and below for Refs. [118] and [106] with EoS-A. The latter improves when increasing the fireball expansion as in the right panel of Fig. 20. Also note that comparing minimum-bias data to calculations at an average $N_{\rm ch}$ underestimates the theoretical contributions which scale with $N_{\rm coll}$ (DY and primordial ρ's).

4.2.3 CERN-SPS II: CERES/NA45 and WA98

The refinements in the analysis of the NA60 dimuon spectra (fireball evolution and additional sources) have been rechecked against existing and updated EM data at the SPS.

The updated calculations of Ref. [106] agree well with the combined '95/'96 CERES dielectron data (left panel of Fig. 22). For the 2000 data (right panel of Fig. 22), the cocktail-subtracted excess spectra in central Pb-Au corroborate the main findings of the NA60 data, i.e., a quantitative agreement with the in-medium ρ of Ref. [30] and the predominance of baryon effects. The longer lifetime of the fireball in central Pb-Au (factor

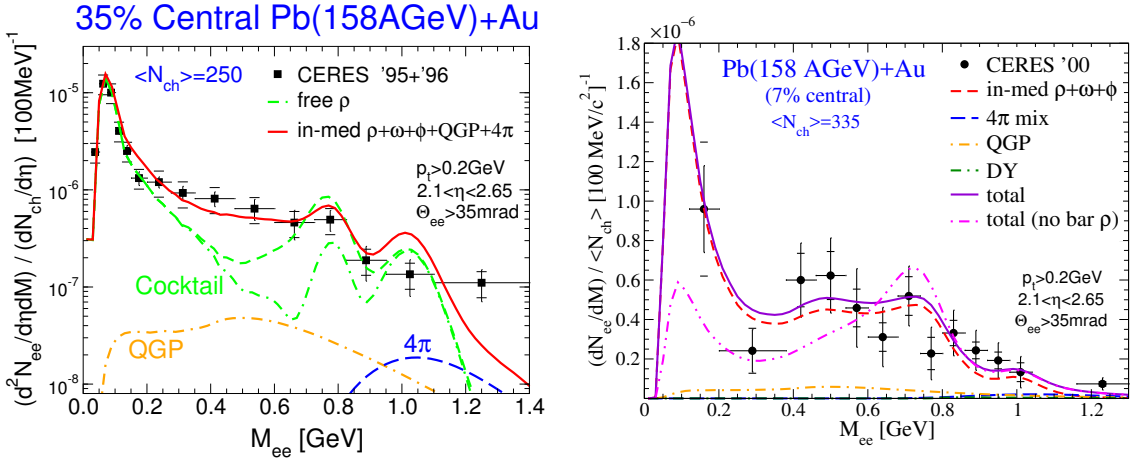

Figure 22: *CERES/NA45 data for e^+e^- invariant-mass spectra in* Pb(158 AGeV)-Au *collisions at the SPS [32, 37]. The left panel corresponds to semicentral collisions including the contribution from long-lived hadron decays after freeze-out ("cocktail", dash-dotted line), while the right panel shows "excess" spectra for central collisions. The theoretical predictions are based on in-medium ρ spectral functions [30] supplemented by ω and ϕ decays, as well as Drell-Yan and 4π annihilation [106] (as for the NA60 data, see Fig. 17).*

$\sim$2 relative to In-In) reduces the uncertainties due to ρ-meson cocktail contributions. In addition, dielectrons enable access to very low masses, where the '00 CERES data may bear a first hint of a large enhancement as predicted by hadronic many-body theory.

As emphasized in Sec. 3.5, (very) low-mass dilepton rates are intimately related to thermal photon spectra. In Ref. [108] the in-medium ρ spectral function of Ref. [30] has been carried to the photon point and convoluted over the same fireball expansion as before; when supplemented with t-channel exchange reactions, QGP emission and primordial (hard) photons constrained by p-A data, the resulting q_t spectra are consistent with WA98 photon spectra, see lower right panel of Fig. 23; the updated fireball evolution barely affects the total spectra. The contributions from the lightlike ρ are prevalent up to $q_t \simeq 1$ GeV (cf. Fig. 15), after which t-channel processes takes over. Primordial photons outshine the combined thermal yield (hadronic+QGP) for $q_t \gtrsim 2$ GeV. This is nicely consistent with the calculations of Ref. [149], see lower left panel in Fig. 23. In earlier calculations of Refs. [148, 126] the thermal yield is significantly larger, due to an increased QGP contribution caused by a short formation time of τ_0=0.2-0.33 fm/c with associated peak temperatures of up to T_0=335 MeV (for τ_0=1 fm/c [108, 149] average initial temperatures are slightly above $\bar{T}_0$=200 MeV). Even for this upper estimate of QGP emission[12], the latter is smaller than the hadronic one for momenta $q_t \leq$1.5-2 GeV, and the pQCD photons are at the $\sim$40% level of the combined thermal contribution at $q_t \simeq 2$ GeV.

Similar conclusions arise from theoretical analyses [140, 150, 151] of intermediate-mass dimuon spectra ($1.5 \geq M_{\mu\mu}/\mathrm{GeV} < 3$) in Pb-Pb collisions at SPS [152]: unless the initial temperature significantly exceeds T_0=250 MeV, the thermal contribution falls below primoridial sources (DY) at masses and transverse momenta beyond $M, q_t \simeq$1.5-2 GeV. This is fully confirmed by the recent NA60 intermediate-mass dilepton spectra [137].

[12] At SPS energy, with a Lorentz contraction of $\gamma \simeq 9$ for the incoming nuclei, the time for full nuclear overlap is ca. 0.8 fm/c.

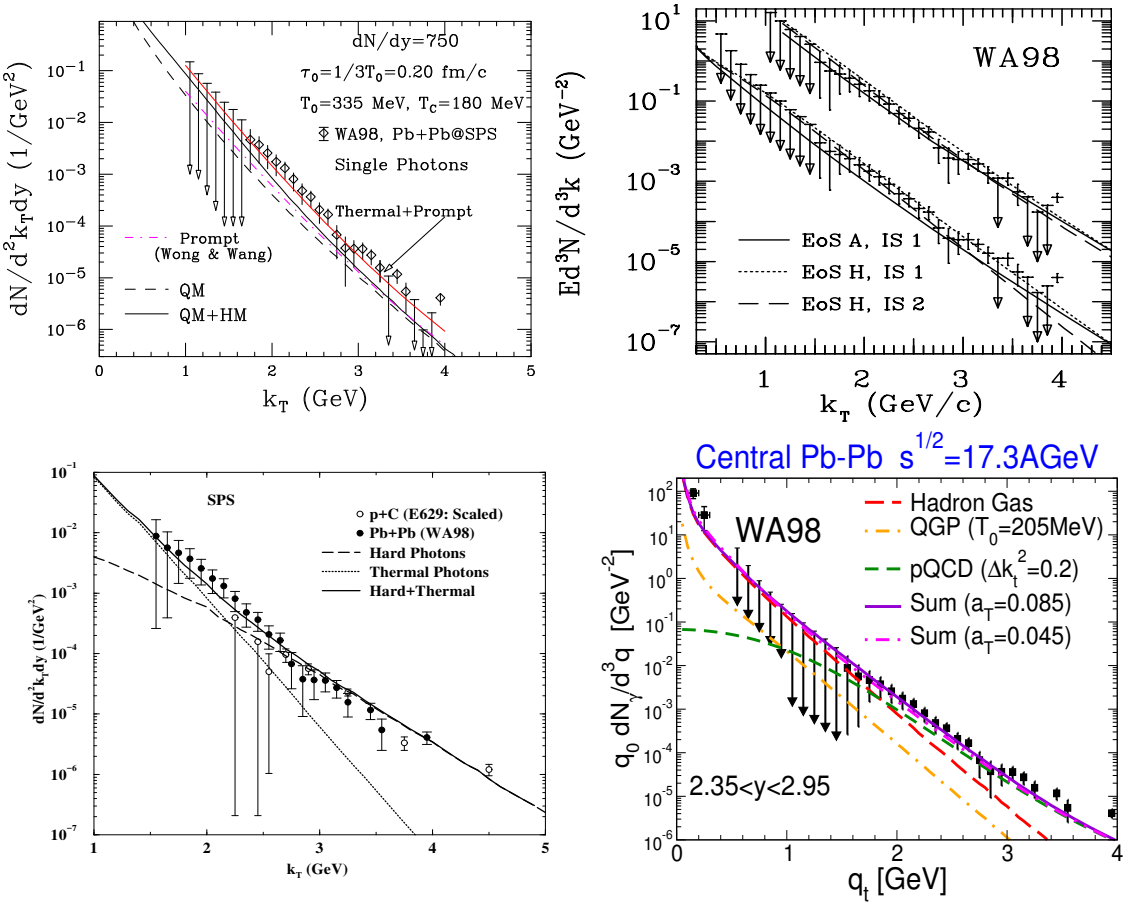

Figure 23: *Direct photon spectra in central* Pb(158 AGeV)-Pb *collisions at the SPS as measured by the WA98 collaboration [146, 147]. The upper panels contain theoretical calculations [148, 126] with a moderate primordial pQCD component and a hot initial state (τ_0=0.2-0.33 fm/c; in the upper left panel the lower curves are without primordial emission), while the calculations in the lower panels [149, 108] contain primordial emission with Cronin effect and a larger thermalization time ($\tau_0 \simeq 1$ fm/c).*

4.2.4 Future Dilepton Measurements

Dilepton programs will be pursued with high priority over a wide range of collision energies. The large enhancement observed in a low-energy (40 AGeV) run at SPS [38] is in line with the prediction of hadronic-many body theory that medium effects caused by baryons play a leading role [70]. This trend continues down to much lower bombarding energies of 1-2 AGeV. However, at these energies recent transport calculations suggest that the low-mass enhancement, which could not be explained by hadronic in-medium effects [27], is related to primordial N-N Bremsstrahlung [153], as well as $\Delta \to N e^+ e^-$ and η Dalitz decays [154, 155]. A better sensitivity to medium effects appears to be in the ρ-ω mass region, where the (lack of) yield indicates a strong broadening of the vector resonances [156, 154, 157].

At the high-energy frontier, first RHIC data [42] find a large e^+e^- signal especially in the mass region around $M \simeq 0.3$ GeV. The excess is concentrated at low q_t and in central collisions, and cannot be explained by current in-medium spectral functions. It is tempting to speculate that the excess is caused by the formation of a disoriented chiral condensate

(DCC), as pion-DCC annihilation shares the above features [158]. However, the magnitude of this dilepton source cannot easily compete with hadronic medium effects, unless the DCC domains are rather large and abundant. In this case, footprints of the DCC should be visible in other observables (e.g., π^0 and p_T fluctuations). Precision measurements within the RHIC-II program will be of crucial importance here [43].

Finally, dilepton data will play a critical role in the CBM experiment at the future GSI facility (FAIR). In the planned energy regime, $E_{\rm lab}$=10-40 AGeV, one envisages the largest nuclear compression and thus maximal baryon density, ideally suited to scrutinize the current understanding of medium effects. An extra benefit could be the occurence of a critical point or a true mixed phase at a first-order transition, with extended fireball lifetimes further enhancing the dilepton signal.

4.3 Critical Appraisal

In this section we evaluate the current status of determining the in-medium vector spectral functions (focusing on the ρ meson) and the implications for chiral restoration.

Calculations of ρ-meson spectral functions based on effective chiral Lagrangians coupled with many-body techniques agree on a strong broadening with small (positive) mass shifts. At normal nuclear matter density, one finds an increase in width of $\Delta\Gamma_\rho \simeq 250\,$MeV with an estimated error of $\sim$30%, i.e., the vacuum width almost triples. The question whether the parameters in the effective Lagrangian are subject to in-medium changes requires further input. In the vector-manifestation scenario, reduced bare masses and coupling constants are inferred from a matching of the correlators to an operator product expansion (OPE) at spacelike momenta governed by the in-medium reduction of the condensates. However, it turns out that, within current uncertainties, the softening of the ρ spectral function as imposed by the OPE at nuclear matter density is fully accounted for by the broadening due to hadronic many-body effects. More accurate tests of this assertion, especially at higher densities/temperatures, will require a more precise determination of the in-medium condensates on the OPE side of the QCD sum rule. The predicted broadening is supported by several recent experiments where dilepton spectra have been measured with impressive precision: at JLAB, photoproduction data off mid-size nuclei find a ρ broadening of $\Delta\Gamma_\rho^{\rm NUC} \simeq$70-100 MeV without significant mass shift, consistent with many-body effects at about half nuclear density and 3-momenta of $\sim$1-2 GeV. The NA60 dilepton spectra in central In-In collisions exhibit an *average* ρ width of $\bar{\Gamma}_\rho^{\rm HIC} \simeq 400\,$MeV i.e., an additional broadening of $\Delta\bar{\Gamma}_\rho^{\rm HIC} \simeq 250\,$MeV. Typical kinetic freeze-out conditions at SPS energies are $(\rho_B^{\rm fo}, T_{\rm fo}) \simeq (0.3\rho_0, 120{\rm MeV})$. With initial temperatures of $T_0 \simeq 200\,$MeV (as suggested by "effective" slope parameters in the q_T spectra for M>1 GeV, as well as direct photon spectra in Pb-Pb), the average ρ width thus reflects the medium at an average temperature of $\bar{T} \simeq 150\,$MeV (the growing fireball 3-volume "biases" low-mass dilepton radiation to more dilute stages). This implies that the ρ width approaches its mass when the system moves toward the (pseudo) critical temperature, $\Gamma_\rho(T \to T_c) \to m_\rho$, i.e., the resonance "melts" (see also Ref. [159]). Inspection of the theoretical predictions for the width of the ρ as extracted from the vector spectral function corroborates this conclusion, cf. Fig. 24. The circumstantial "duality" of hadronic and partonic EM emission rates close to T_c lends robustness to the pertinent predictions for dilepton spectra in heavy-ion collisions as they become independent on details of the evolution model, in particular of the treatment of the phase transition region. The excess radiation at intermediate mass, with its rather soft emission characteristics in q_t, as well as direct photon spectra, further

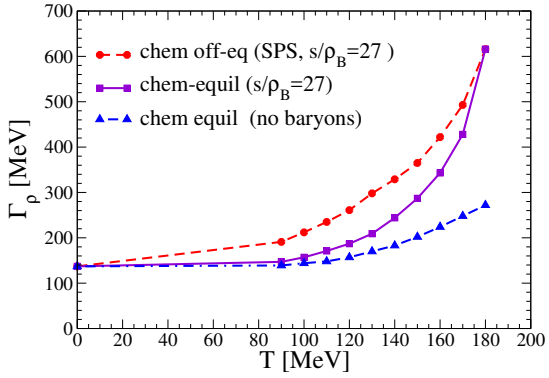

Figure 24: *Temperature dependence of the ρ width as evaluated in hadronic many-body theory [30] at fixed entropy per baryon representative for heavy-ion collisions at full SPS energy (dashed and solid line: with and without meson chemical potentials). For the dash-dotted line, medium effects due to baryons are switched off.*

consolidate the origin of thermal radiation from around T_c.

A no less challenging task is to connect the above findings to the chiral transition. It has recently been argued that the statistical operator consisting of a (free) hadron resonance gas (HRG) is capable of reproducing several features of lattice QCD computations of the equation of state (EoS) until rather close to the (pseudo-) critical temperature [160, 161]. Beyond T_c the lattice EoS levels off, reflecting quark-gluon degrees of freedom, while the HRG EoS diverges (Hagedorn catastrophe). The ρ melting offers a microscopic explanation for this transition: under moderate conditions, the *interacting* HRG physics drives the ρ broadening to an extent which justifies the use of well-defined quasi-particle states in the statistical operator. With further increasing temperature and density, resonance overlap in the ρ spectral function drives it to a continuum shape *with a strength resembling a weakly interacting $q\bar{q}$ pair*, i.e., the resonance strength in the statistical operator converts into partonic strength. The phenomenon of overlapping resonances merging into a perturbative $q\bar{q}$ continuum is, of course, well known from the e^+e^- annihilation cross section into hadrons above $M\simeq$1.5 GeV. It is suggestive that the thermal medium provides the necessary phase space for low-mass resonances which, via their mutual "mixing" in different hadronic correlators, "restore" quark-hadron duality down to $M\to 0$, implying chiral restoration. To quantify this picture the evaluation of chiral order parameters is mandatory. It is tempting to speculate that the rather sharp increase of the ρ width close to the expected critical temperature (especially in chemical equilibrium as realized in lattice QCD, represented by the solid line in Fig. 24) is signaling the chiral transition. QCD sum rules remain a valuable tool if the T (and μ_B) dependence of the quark and gluon condensates can be made more precise. Ideally, the latter are determined from first-principle lattice QCD calculations. Possibly the most promising approach, which has been little exploited thus far, are chiral (or Weinberg) sum rules. Their use hinges on the in-medium axialvector spectral function. The latter is much more difficult to constrain due to a principal lack of experimental information, encoded in either 3-pion or π-γ final states. This stipulates the importance of calculating the axialvector correlator in chiral models. In connection with a realistic vector correlator and lattice-QCD input on the in-medium condensates, the explicit realization of chiral restoration can be investigated. First efforts in this direction have been undertaken [162, 163, 164, 165], but a full treatment including quantitative V and A spectral functions, even in the vacuum, is currently lacking.

5 Conclusions

Medium modifications of hadronic spectral functions play a key role in the diagnosis of hot/dense strongly interacting matter and its condensate structure. Experimentally, the most promising approach is dilepton spectroscopy which directly probes the vector spectral function of the hadronic medium. For the ρ-meson, which dominates the low-mass vector channel, effective hadronic theories largely agree on a strong broadening of the resonance, with little mass shift. Baryon effects prevail over those induced by mesons, and the predicted modifications in cold nuclear matter are compatible with QCD sum rules at finite density. Intense experimental efforts over the last $\sim$15 years have culminated to a new level of precision which broadly confirms the theoretical expectations: production experiments off ground-state nuclei find an increase of the ρ width by $\sim$80 MeV, while the effect in heavy-ion collisions at the SPS is by a factor of $\sim$3 larger. Part of this difference is due to the access to the low-momentum regime in the heavy-ion measurements. It is therefore highly desirable to push the sensitivity of the nuclear experiments to low 3-momenta where significantly larger medium effects are predicted. The average ρ width extracted in heavy-ion collisions suggests that the ρ resonance "melts" close to the expected phase boundary, in agreement with extrapolations of hadronic models. This is a first explicit evidence that melting resonances are involved in the transition from hadronic to quark degrees of freedom. Modern quark-model calculations could provide complementary insights when approaching T_c from above. Unquenched lattice QCD computations of the vector correlator would undoubtedly set valuable benchmarks and possibly shed light on the conjecture that the width is connected to order parameters of chiral symmetry restoration. In addition, information on quark condensates and pion decay constant(s) below T_c can be connected to hadronic vector and axialvector spectral functions utilizing Weinberg sum rules. The synergy of hadronic and quark models with first-principle lattice QCD computations, augmented by quantitative applications to experiment at current and future facilities, opens exciting perspectives to improve our knowledge about the chiral transition in hot/dense QCD matter and the generation of luminous mass in the Universe.

Acknowledgments

We thank H.J. Specht and S. Damjanovic for valuable discussions and suggestions. RR has been supported by a U.S. National Science Foundation CAREER Award under grant PHY-0449489, and by the A. v. Humboldt-Foundation through a Bessel Research Award.

References

[1] E.V. Shuryak, *The QCD Vacuum, Hadrons and Superdense Matter*, 2. edition, World Scientific Lecture Notes in Physics, Vol. **71** (2004).

[2] P. Braun-Munzinger and J. Wambach, `arXiv:0801.4256[hep-ph]`.

[3] L. Y. Glozman, Phys. Rept. **444**, 1 (2007).

[4] M. Cheng *et al.*, Phys. Rev. D **74**, 054507 (2006).

[5] Y. Aoki, Z. Fodor, S. D. Katz, and K. K. Szabo, Phys. Lett. B **643**, 46 (2006).

[6] U. W. Heinz and M. Jacob (2000), arXiv:nucl-th/0002042.

[7] I. Arsene *et al.* (BRAHMS Collaboration), Nucl. Phys. A **757**, 1 (2005);
B.B. Back *et al.* (PHOBOS Collaboration), *ibid.* 28 (2005);
J. Adams *et al.* (STAR Collaboration), *ibid.* 102 (2005);
K. Adcox *et al.* (PHENIX Collaboration), *ibid.* 184 (2005).

[8] P. Braun-Munzinger, K. Redlich and J. Stachel (2003), in R.C. Hwa, X.N. Wang (editors), *Quark-gluon plasma* vol. 3 (World Scientific, 2004) p491, arXiv:nucl-th/0304013.

[9] F. Becattini, M. Gazdzicki, A. Keranen, J. Manninen and R. Stock, Phys. Rev. C **69**, 024905 (2004); F. Becattini, J. Manninen, and M. Gazdzicki, Phys. Rev. C **73**, 044905 (2006).

[10] D. Teaney, J. Lauret, and E. V. Shuryak (2001), arXiv:nucl-th/0110037.

[11] T. Hirano and K. Tsuda, Phys. Rev. C **66**, 054905 (2002).

[12] P. F. Kolb and U. W. Heinz (2003), published in R.C. Hwa, X.N. Wang (editors), *Quark-gluon plasma* vol. 3 (World Scientific, 2004) p634, arXiv:nucl-th/0305084.

[13] C. Nonaka and S. A. Bass, Phys. Rev. C **75**, 014902 (2007).

[14] A. Adare *et al.* (PHENIX Collaboration), Phys. Rev. Lett. **98**, 162301 (2007).

[15] B. I. Abelev *et al.* (STAR Collaboration), Phys. Rev. C **75**, 054906 (2007).

[16] E. L. Feinberg, Nuovo Cim. A **34**, 391 (1976).

[17] E. V. Shuryak, Phys. Lett. B **78**, 150 (1978).

[18] L. D. McLerran and T. Toimela, Phys. Rev. D **31**, 545 (1985).

[19] J. J. Sakurai, *Currents and Mesons* (University of Chicago Press, Chicago, 1969).

[20] R. Rapp, J. Phys. G **31**, S217 (2005).

[21] G.E. Brown and M. Rho, Phys. Rev. Lett. **66**, 2720 (1991); Phys. Rept. **269**, 333 (1996).

[22] G. Agakishiev *et al.* (CERES/NA45 Collaboration), Phys. Rev. Lett. **75**, 1272 (1995).

[23] G.-Q. Li, C. M. Ko, and G. E. Brown, Phys. Rev. Lett. **75**, 4007 (1995).

[24] W. Cassing, W. Ehehalt, and C. M. Ko, Phys. Lett. B **363**, 35 (1995).

[25] R. Rapp and J. Wambach, Adv. Nucl. Phys. **25**, 1 (2000).

[26] J. Alam, S. Sarkar, P. Roy, T. Hatsuda, and B. Sinha, Annals Phys. **286**, 159 (2001).

[27] W. Cassing and E. L. Bratkovskaya, Phys. Rept. **308**, 65 (1999).

[28] C. Gale and K. L. Haglin (2003), in R. C. Hwa, X. N. Wang (editors), *Quark-gluon plasma* vol. 3 (World Scientific, 2004) p364, arXiv:hep-ph/0306098.

[29] R. Rapp, G. Chanfray, and J. Wambach, Nucl. Phys. A **617**, 472 (1997).

[30] R. Rapp and J. Wambach, Eur. Phys. J. A **6**, 415 (1999).

[31] G. Agakishiev *et al.* (CERES/NA45 Collaboration), Phys. Lett. B **422**, 405 (1998).

[32] G. Agakichiev *et al.* (CERES/NA45 Collaboration), Eur. Phys. J. C **41**, 475 (2005).

[33] S. Bethke, Prog. Part. Nucl. Phys. **58**, 351 (2007).

[34] R. Rapp, Nucl. Phys. A **661**, 33 (1999).

[35] R. Arnaldi *et al.* (NA60 Collaboration), Phys. Rev. Lett. **96**, 162302 (2006).

[36] H. van Hees and R. Rapp, Phys. Rev. Lett. **97**, 102301 (2006).

[37] D. Adamova *et al.* (CERES/NA45 Collaboration), Phys. Lett. B **666**, 425 (2008).

[38] D. Adamova *et al.* (CERES/NA45 Collaboration), Phys. Rev. Lett. **91**, 042301 (2003).

[39] R. J. Porter *et al.* (DLS Collaboration), Phys. Rev. Lett. **79**, 1229 (1997).

[40] G. Agakichiev *et al.* (HADES Collaboration), Phys. Rev. Lett. **98**, 052302 (2007).

[41] G. Agakishiev *et al.* (HADES Collaboration), Phys. Lett. B **663**, 43 (2008).

[42] S. Afanasiev *et al.* (PHENIX Collaboration) (2007), `arXiv:0706.3034[nucl-ex]`.

[43] G. David, R. Rapp, and Z. Xu, Phys. Rept. **462**, 176 (2008).

[44] D. Trnka *et al.* (CBELSA/TAPS Collaboration), Phys. Rev. Lett. **94**, 192303 (2005).

[45] R. Nasseripour *et al.* (CLAS Collaboration), Phys. Rev. Lett. **99**, 262302 (2007).

[46] M. Naruki *et al.* (E325 Collaboration), Phys. Rev. Lett. **96**, 092301 (2006).

[47] H. Fritzsch, M. Gell-Mann and H. Leutwyler, Phys. Lett. B **47**, 365 (1973).

[48] D. J. Gross and F. Wilczek, Phys. Rev. Lett. **30**, 1343 (1973).

[49] H. D. Politzer, Phys. Rev. Lett. **30**, 1346 (1973).

[50] R. Barate *et al.* (ALEPH Collaboration), Eur. Phys. J. C **4**, 409 (1998).

[51] K. Ackerstaff *et al.* (OPAL Collaboration), Eur. Phys. J. C **7**, 571 (1999).

[52] S. Weinberg, Phys. Rev. Lett. **18**, 507 (1967).

[53] T. Das, V. S. Mathur, and S. Okubo, Phys. Rev. Lett. **19**, 859 (1967).

[54] H. Leutwyler, *Restoration of Chiral Symmetry*, In *Dobogokoe 1991, Proceedings, Effective field theories of the standard model* 193-224.

[55] E. G. Drukarev and E. M. Levin, Prog. Part. Nucl. Phys. **27**, 77 (1991).

[56] T. D. Cohen, R. J. Furnstahl, and D. K. Griegel, Phys. Rev. C **45**, 1881 (1992).

[57] S. Zschocke, B. Kämpfer, O. P. Pavlenko, and G. Wolf (2002), arXiv:nucl-th/0202066.

[58] M. Cheng *et al.*, Phys. Rev. D **77**, 014511 (2008).

[59] D. E. Miller, Phys. Rept. **443**, 55 (2007).

[60] T. Hatsuda and T. Kunihiro, Phys. Rev. Lett. **55**, 158 (1985).

[61] G. E. Brown, C.-H. Lee, M. Rho, and E. Shuryak, Nucl. Phys. A **740**, 171 (2004).

[62] M. Mannarelli and R. Rapp, Phys. Rev. C **72**, 064905 (2005).

[63] A. Starostin *et al.* (Crystal Ball Collaboration), Phys. Rev. Lett. **85**, 5539 (2000).

[64] N. Grion *et al.* (CHAOS Collaboration), Nucl. Phys. A **763**, 80 (2005).

[65] F. Bloch *et al.*, Eur. Phys. J. A **32**, 219 (2007).

[66] T. Hatsuda, T. Kunihiro, and H. Shimizu, Phys. Rev. Lett. **82**, 2840 (1999).

[67] R. Rapp *et al.*, Phys. Rev. C **59**, 1237 (1999).

[68] M. J. Vicente Vacas and E. Oset, Phys. Rev. C **60**, 064621 (1999).

[69] O. Buss, L. Alvarez-Ruso, A.B. Larionov, and U. Mosel, Phys. Rev. C **74**, 044610 (2006).

[70] R. Rapp, Pramana **60**, 675 (2003).

[71] M. Dey, V. L. Eletsky, and B. L. Ioffe, Phys. Lett. B **252**, 620 (1990).

[72] B. Krippa, Phys. Lett. B **427**, 13 (1998).

[73] G. Chanfray, J. Delorme, M. Ericson and M. Rosa-Clot, Phys. Lett. B **455**, 39 (1999).

[74] J. V. Steele, H. Yamagishi, and I. Zahed, Phys. Lett. B **384**, 255 (1996).

[75] J. V. Steele, H. Yamagishi, and I. Zahed, Phys. Rev. D **56**, 5605 (1997).

[76] J. V. Steele and I. Zahed, Phys. Rev. D **60**, 037502 (1999).

[77] F. Karsch, E. Laermann, P. Petreczky, S. Stickan, and I. Wetzorke, Phys. Lett. B **530**, 147 (2002).

[78] E. Braaten, R. D. Pisarski, and T.-C. Yuan, Phys. Rev. Lett. **64**, 2242 (1990).

[79] M. Asakawa, T. Hatsuda, and Y. Nakahara, Prog. Part. Nucl. Phys. **46**, 459 (2001).

[80] G. D. Moore and J.-M. Robert (2006), arXiv:hep-ph/0607172.

[81] C. R. Allton *et al.*, Phys. Rev. D **71**, 054508 (2005).

[82] J.I. Kapusta and E.V. Shuryak, Phys. Rev. D **49**, 4694 (1994).

[83] M. A. Shifman, A. I. Vainshtein, and V. I. Zakharov, Nucl. Phys. B **147**, 385 (1979).

[84] T. Hatsuda and S. H. Lee, Phys. Rev. C **46**, 34 (1992).

[85] M. Asakawa and C. M. Ko, Nucl. Phys. A **560**, 399 (1993).

[86] F. Klingl, N. Kaiser and W. Weise, Nucl. Phys. A **624**, 527 (1997).

[87] S. Leupold, W. Peters and U. Mosel, Nucl. Phys. A **628**, 311 (1998).

[88] J. Ruppert, T. Renk and B. Müller, Phys. Rev. C **73**, 034907 (2006).

[89] Y. Kwon, M. Procura and W. Weise, `arXiv:0803.3262[nucl-th]`.

[90] M. Bando, T. Kugo, S. Uehara, K. Yamawaki, and T. Yanagida, Phys. Rev. Lett. **54**, 1215 (1985).

[91] H. Gomm, O. Kaymakcalan, and J. Schechter, Phys. Rev. D **30**, 2345 (1984).

[92] M. Harada and K. Yamawaki, Phys. Rept. **381**, 1 (2003).

[93] M. Harada and C. Sasaki, Phys. Rev. D **74**, 114006 (2006)

[94] M. Urban, M. Buballa, R. Rapp, and J. Wambach, Nucl. Phys. A **673**, 357 (2000).

[95] C. Song, Phys. Rev. D **53**, 3962 (1996).

[96] R. Rapp and C. Gale, Phys. Rev. C **60**, 024903 (1999).

[97] A. Dobado, A. Gomez Nicola, F. J. Llanes-Estrada and J. R. Pelaez, Phys. Rev. C **66**, 055201 (2002)

[98] K. Haglin, Nucl. Phys. A **584**, 719 (1995)

[99] V.L. Eletsky, M. Belkacem, P.J. Ellis and J.I. Kapusta, Phys. Rev. C **64**, 035202 (2001).

[100] M. Post, S. Leupold, and U. Mosel, Nucl. Phys. A **741**, 81 (2004).

[101] D.M. Manley, R.A. Arndt, Y. Goradia and V.L. Teplitz, Phys. Rev. D **30**, 904 (1984).

[102] T.P. Vrana, S.A. Dytman, and T.S.H. Lee, Phys. Rept. **328**, 181 (2000).

[103] R. Rapp, M. Urban, M. Buballa, and J. Wambach, Phys. Lett. B **417**, 1 (1998).

[104] M. F. M. Lutz, G. Wolf, and B. Friman, Nucl. Phys. A **706**, 431 (2002).

[105] R. Rapp, Phys. Rev. C **63**, 054907 (2001).

[106] H. van Hees and R. Rapp, Nucl. Phys. A **806**, 339 (2008).

[107] R. Rapp (2002), `arXiv:nucl-th/0204003`.

[108] S. Turbide, R. Rapp, and C. Gale, Phys. Rev. C **69**, 014903 (2004).

[109] J. I. Kapusta, P. Lichard and D. Seibert, Phys. Rev. D **44**, 2774 (1991) [Erratum-ibid. D **47**, 4171 (1993)].

[110] P. Arnold, G. D. Moore, and L. G. Yaffe, JHEP **0112**, 009 (2001).

[111] M. H. Wood *et al.* [CLAS Collaboration], Phys. Rev. C **78**, 015201 (2008).

[112] F. Riek, R. Rapp, T. S. Lee and Y. Oh, arXiv:0812.0987[nucl-th].

[113] G. M. Huber *et al.* (TAGX Collaboration), Phys. Rev. C **68**, 065202 (2003).

[114] W. Cassing, E. L. Bratkovskaya, R. Rapp and J. Wambach, Phys. Rev. C **57**, 916 (1998).

[115] P. Huovinen, M. Belkacem, P. J. Ellis and J. I. Kapusta, Phys. Rev. C **66**, 014903 (2002).

[116] E. L. Bratkovskaya, W. Cassing and O. Linnyk, arXiv:0805.3177[nucl-th].

[117] K. Dusling, D. Teaney, and I. Zahed, Phys. Rev. C **75**, 024908 (2007).

[118] K. Dusling and I. Zahed (2007), arXiv:hep-ph/0701253.

[119] T. Renk and J. Ruppert, Phys. Rev. C **77**, 024907 (2008).

[120] J. Ruppert, C. Gale, T. Renk, P. Lichard, and J. I. Kapusta, Phys. Rev. Lett. **100**, 162301 (2008).

[121] I. G. Bearden *et al.* (NA44 Collaboration), Phys. Rev. Lett. **78**, 2080 (1997).

[122] H. Appelshäuser *et al.* (NA49 Collaboration), Eur. Phys. J. C **2**, 661 (1998).

[123] F. Antinori *et al.* (WA97 Collaboration), J. Phys. G **27**, 2325 (2001); J. Phys. G **33**, 403 (2007).

[124] D. Adamova *et al.* (CERES Collaboration), Nucl. Phys. A **714**, 124 (2003).

[125] V.V. Skokov and V.D. Toneev, Phys. Rev. C **73**, 021902 (2006).

[126] P. Huovinen, P. V. Ruuskanen and S. S. Räsanen, Phys. Lett. B **535**, 109 (2002).

[127] C. Alt *et al.* [NA49 Collaboration], Phys. Rev. C **68**, 034903 (2003).

[128] J.P. Wurm, J. Bielcikova [CERES/NA45 Collaboration], arXiv:nucl-ex/0407019.

[129] R. Rapp, Phys. Rev. C **66**, 017901 (2002).

[130] D. Teaney, arXiv:nucl-th/0204023.

[131] R. Rapp, H. van Hees and T. Strong, Braz. J. Phys. **37**, 779 (2007).

[132] F. Cooper and G. Frye, Phys. Rev. D **10**, 186 (1974).

[133] J. Knoll (2008), arXiv:0803.2343[nucl-th].

[134] W. Cassing and E. L. Bratkovskaya (2008), arXiv:0808.0022[hep-ph].

[135] D. d'Enterria, Eur. Phys. J. C **43**, 295 (2005).

[136] F. Halzen and D. M. Scott, Phys. Rev. D **18**, 3378 (1978).

[137] R. Arnaldi *et al.* [NA60 Collaboration], arXiv:0810.3204[nucl-ex].

[138] R. Arnaldi *et al.* [NA60 Collaboration], arXiv:0812.3053[nucl-ex].

[139] T. Sjostrand, P. Eden, C. Friberg, L. Lonnblad, G. Miu, S. Mrenna and E. Norrbin, Comput. Phys. Commun. **135**, 238 (2001).

[140] R. Rapp and E. V. Shuryak, Phys. Lett. B **473**, 13 (2000).

[141] S. Damjanovic *et al.* (NA60 Collaboration), Nucl. Phys. A **783**, 327 (2007).

[142] R. Arnaldi *et al.* (NA60 Collaboration), Phys. Rev. Lett. **100**, 022302 (2008).

[143] T. Renk, R. A. Schneider and W. Weise, Phys. Rev. C **66**, 014902 (2002).

[144] P. Lichard and J. Juran, Phys. Rev. D **76**, 094030 (2007).

[145] S. Damjanovic *et al.* [NA60 Collaboration], J. Phys. G **35**, 104036 (2008).

[146] M. M. Aggarwal *et al.* (WA98 Collaboration), Phys. Rev. Lett. **85**, 3595 (2000).

[147] M.M. Aggarwal *et al.* (WA98 Collaboration), Phys. Rev. Lett. **93**, 022301 (2004).

[148] D.K. Srivastava and B. Sinha, Phys. Rev. C **64**, 034902 (2001).

[149] J. Alam, B. Mohanty, P. Roy, S. Sarkar, and B. Sinha, Phys. Rev. C **67**, 054902 (2003).

[150] K. Gallmeister, B. Kampfer and O. P. Pavlenko, Phys. Lett. B **473**, 20 (2000).

[151] I. Kvasnikova, C. Gale and D. K. Srivastava, Phys. Rev. C **65**, 064903 (2002).

[152] M. C. Abreu *et al.* (NA38 Collaboration), Eur. Phys. J. C **14**, 443 (2000).

[153] F. de Jong and U. Mosel, Phys. Lett. B **392**, 273 (1997).

[154] E.L. Bratkovskaya and W. Cassing, Nucl. Phys. A **807**, 214 (2008).

[155] D. Schumacher, S. Vogel and M. Bleicher, Acta Phys. Hung. A **27**, 451 (2006).

[156] K. Shekhter, C. Fuchs, A. Faessler, M. Krivoruchenko and B. Martemyanov, Phys. Rev. C **68**, 014904 (2003).

[157] E. Santini *et al.*, Phys. Rev. C **78**, 034910 (2008).

[158] Y. Kluger, V. Koch, J. Randrup and X.N. Wang, Phys. Rev. C **57**, 280 (1998).

[159] C. A. Dominguez and M. Loewe, Z. Phys. C **49**, 423 (1991).

[160] F. Karsch, K. Redlich and A. Tawfik, Phys. Lett. B **571**, 67 (2003).

[161] S. Ejiri, F. Karsch and K. Redlich, Phys. Lett. B **633**, 275 (2006).

[162] R. Rapp, Eur. Phys. J. A **18**, 459 (2003).

[163] M. Harada and C. Sasaki, Phys. Rev. D **73**, 036001 (2006).

[164] S. Strüber and D. H. Rischke, Phys. Rev. D **77**, 085004 (2008).

[165] M. Harada, C. Sasaki and W. Weise, arXiv:0807.1417[hep-ph].